EFFECT OF TEMPERATURE ON MECHANICAL PROPERTIES OF NANOCLAY REINFORCED POLYMERIC NANOCOMPOSITES – PART II: MODELING AND THEORETICAL PREDICTIONS*

by

S. Bayar, F. Delale and J. Li

Mechanical Engineering Department

The City College of New York, New York, NY 10031

ABSTRACT

In this paper we present the modeling and theoretical prediction for the results given in Part I [1] for nanoclay reinforced polymers subjected to mechanical and thermal loads. In the previous paper (Part I) the mechanical properties for 3 grades of polypropylene (PP) and epoxy reinforced with nanoclay were experimentally determined at various temperatures. In this study using the Mori-Tanaka formulations (for oriented particles, 2-D randomly distributed particles and 3-D randomly distributed particles) and the Finite Element Method (FEM) the Young's modulus and Poisson's ratio are calculated and then compared with the experimental results. The Mori-Tanaka formulation is modified to take into account nanoclay particles of varying dimensions and also the effect of voids. In addition at high temperatures, the formulation is further modified to include the effect of temperature in the calculation of the Young's modulus. It is found that the results obtained from the modified Mori-Tanaka calculations compare well with the experimental results. The Finite Element calculations also provide a reasonable estimate for the Young's modulus, but the results are less predictive than the Mori-Tanaka results.

1- INTRODUCTION

In the previous paper (Part I), the experimental results obtained for nanoclay reinforced three grades of PP and epoxy at various temperatures were presented. Specifically, the variation of mechanical properties (such as Young's modulus, Poisson's ratio, ultimate stress, failure or end of test strain) with temperature and nanoclay reinforcement percentage was discussed in detail. In this paper (Part II) using a modified Mori-Tanaka formulation and the Finite Element Method, the Young's modulus and the Poisson's ratio are calculated and compared with their counterpart obtained experimentally.

Compared to experimental studies, the number of publications dealing with theoretical prediction of properties in polymer/clay nanocomposites is relatively small. As reported in [2] some continuum-mechanics based theoretical models to predict the mechanical properties have been proposed [3-6]. Fornes [7] applied the Halpin-Tsai and Mori-Tanaka reinforcement theories to

*This work was supported by US Army-TARDEC under contract #W56HZV-09-C-0569

Report Documentation Page

Form Approved
OMB No. 0704-0188

1. REPORT DATE	2. REPORT TYPE	3. DATES COVERED
22 APR 2012	**Journal Article**	**01-01-2012 to 23-04-2012**

4. TITLE AND SUBTITLE	5a. CONTRACT NUMBER
EFFECT OF TEMPERATURE ON MECHANICAL PROPERTIES OF NANOCLAY REINFORCED POLYMERIC NANOCOMPOSITES - PART II: MODELING AND THEORETICAL PREDICTIONS	**w56hzv-09-c-0569**
	5b. GRANT NUMBER
	5c. PROGRAM ELEMENT NUMBER

6. AUTHOR(S)	5d. PROJECT NUMBER
S Bayar; F Delate; J Li	5e. TASK NUMBER
	5f. WORK UNIT NUMBER

7. PERFORMING ORGANIZATION NAME(S) AND ADDRESS(ES)	8. PERFORMING ORGANIZATION REPORT NUMBER
The City College of New York,Mechanical Engineering Department,160 Convent Avenue,New York,NY,10031	**; #22856**

9. SPONSORING/MONITORING AGENCY NAME(S) AND ADDRESS(ES)	10. SPONSOR/MONITOR'S ACRONYM(S)
U.S. Army TARDEC, 6501 East Eleven Mile Rd, Warren, Mi, 48397-5000	**TARDEC**
	11. SPONSOR/MONITOR'S REPORT NUMBER(S) **#22856**

12. DISTRIBUTION/AVAILABILITY STATEMENT
Approved for public release; distribution unlimited

13. SUPPLEMENTARY NOTES
For the Journal of Composite Materials

14. ABSTRACT

In this paper we present the modeling and theoretical prediction for the results given in Part I [1] for nanoclay reinforced polymers subjected to mechanical and thermal loads. In the previous paper (Part I) the mechanical properties for 3 grades of polypropylene (PP) and epoxy reinforced with nanoclay were experimentally determined at various temperatures. In this study using the Mori-Tanaka formulations (for oriented particles, 2-D randomly distributed particles and 3-D randomly distributed particles) and the Finite Element Method (FEM) the Young?s modulus and Poisson?s ratio are calculated and then compared with the experimental results. The Mori-Tanaka formulation is modified to take into account nanoclay particles of varying dimensions and also the effect of voids. In addition at high temperatures, the formulation is further modified to include the effect of temperature in the calculation of the Young?s modulus. It is found that the results obtained from the modified Mori-Tanaka calculations compare well with the experimental results. The Finite Element calculations also provide a reasonable estimate for the Young?s modulus, but the results are less predictive than the Mori-Tanaka results.

15. SUBJECT TERMS

16. SECURITY CLASSIFICATION OF:			17. LIMITATION OF ABSTRACT	18. NUMBER OF PAGES	19a. NAME OF RESPONSIBLE PERSON
a. REPORT	b. ABSTRACT	c. THIS PAGE			
unclassified	**unclassified**	**unclassified**	**Public Release**	**52**	

predict the modulus of nylon based nanocomposites. The modulus obtained using Mori-Tanaka calculation increased with nanoclay reinforcement as predicted. The Halpin-Tsai formula gave higher values for the modulus but still could be used to predict the value of the modulus. Sheng [2] preformed a more detailed study on theoretical analysis of nanocomposites. A micromechanical model was developed to account for the morphology of the nanocomposite, particle volume fraction, particle aspect ratio, mechanical properties of matrix, exfoliated clay layer thickness and layer spacing. For each case the Halpin-Tsai and Mori-Tanaka models were applied to calculate the variation of the normalized Young's modulus of the nanocomposites with volume fraction, particle aspect ratio, layer thickness and layer spacing. In addition some calculated results were compared with tensile test data. Comparing the Halpin-Tsai and Mori-Tanaka results it was observed that the Mori-Tanaka calculations matched the tensile test data better.

Drozdov [8] studied the viscoelasticity and viscoplasticity of polypropylene/clay nanocomposites. New constitutive equations were developed taking into account the viscoelasticity and viscoplasticity of the nanocomposite and these equations were used in the analysis of the time-dependent response of long-term creep tests. Sheng also presented in [2] an Finite Element model to estimate the Young's modulus of polymer/clay nanocomposites with the representative volume element constructed using TEM observations. The plane strain FEM simulation results for the normalized Young's modulus of the nanocomposite were compared with those obtained from the Mori-Tanaka model and were in good agreement with the experimental data. In [9] the Young's modulus is predicted using the Halpin-Tsai equations and compared with experimental results. The calculated results are much lower than those obtained experimentally. In this study, we introduce a modified Mori-Tanaka formulation to better match the experimental results. First, the calculation from three Mori-Tanaka formulations, namely for oriented particles, 2-D randomly distributed and 3-D randomly distributed particles are presented. The formulation is further refined to account for the effects of voids and temperature. Finally, Finite Element calculations based on the representative volume element concept (RVE) are performed. The comparison of calculated results with those obtained experimentally show that both the Mori-Tanaka formulations and the FEM may be used as effective tools to predict the Young's modulus of nanoclay reinforced PP nanocomposites.

2- THE MORI-TANAKA FORMULATIONS

The purpose of micromechanics modeling of polymer/clay nanocomposites is to predict their elastic properties. For multi-scale modeling, intercalated and exfoliated clay systems were studied. A representative volume element consisting of N layers of intercalated or exfoliated clay platelets surrounded by polymer matrix was considered.

2.1 Application of Mori-Tanaka formulation for tensile testing

To simulate and predict the elastic properties of two-phase nanoclay reinforced nanocomposites we propose to use the Mori-Tanaka model which is based on micromechanics and uses Eshelby's solution for inclusions embedded in an infinite matrix. Here we approximate the nanoclay flakes as thin disks with the aspect ratio α calculated using their thickness and length. For analytical results, three different Mori-Tanaka approaches are used. These approaches depend on particle orientation. The three approaches are: "Oriented particles", "2-D randomly distributed particles" and "3-D randomly distributed particles".

Electron microscopy studies of nanoclay reinforced polymers indicate that (see for example [2,12]) nanoclay particles may be of varying sizes and thicknesses depending on complete or partial exfoliation. Furthermore, they may be randomly distributed with some particles which are oriented. Accordingly, the current nanoclay particle models assume a multi-layer thickness instead of totally exfoliated single flakes. In calculating the particle parameters, here we adopt the model developed by Sheng, et al. [2] which is shown in Figure 1. A similar model is given in [5].

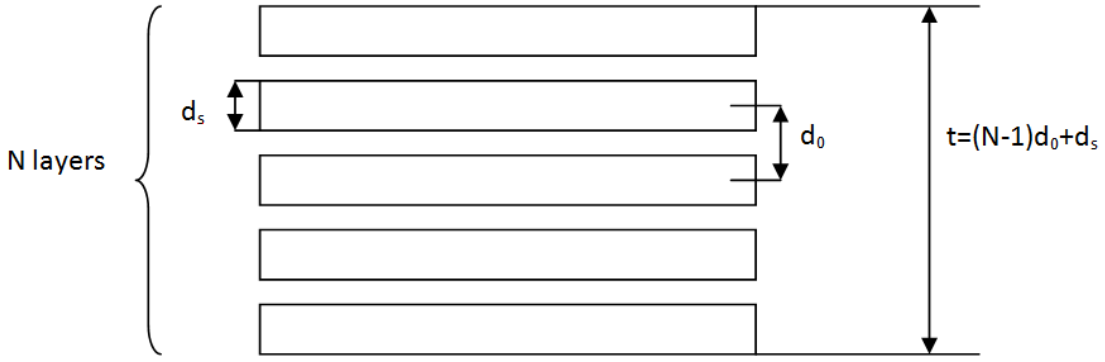

Figure 1. Model of nanoclay particle [2]

In the model it is assumed that the nanoclay particle consists of N flakes of thickness d_s separated by a distance d_0-d_s, where d_0 is the inter-layer spacing. The thickness of the particle can then be calculated as:

$$t = (N-1)d_0 + d_s \qquad (1)$$

In determining the particle thickness for organo-nanoclay we assume an inter-layer spacing for d_0=2.4nm [13] and a flake thickness d_s=0.615nm [2, 14]. Since the size of the particle may vary, here we assume an average diameter of D=200nm.

In the Mori-Tanaka formulas the elastic properties are expressed in terms of the particle volume fraction c. Thus, the reinforcement percentages per weight W_p have to be converted to volume fractions:

$$c = \frac{W_p/\gamma_p}{W_p/\gamma_p + (1 - W_p)/\gamma_p} \tag{2}$$

where W_p, γ_p and γ_m are the weight fraction of nanoclay, specific weight of nanoclay and specific weight of matrix respectively.

For each nanoclay reinforcement, using Eq.2 the volume fraction of nanoclay c is obtained as (Table 1.):

Table 1. Conversion of weight fractions of nanoclay to volume fractions

Weight fraction of nanoclay (W_p)	**Volume fraction of nanoclay (c)**
0.2%	0.095%
1%	0.48%
3%	1.44%
6%	2.93%
10%	5%

Before starting the Mori-Tanaka calculation, we first analyzed the electron microscopy images we obtained for our specimens showing the distribution of nanoclay particles. First, it was noted that not all particles were oriented and they had different sizes. There was also evidence of agglomeration at the higher reinforcement percentages. Thus, any realistic micromechanical model should take into account the different sizes, (including thickness) and distribution patterns of the particles. This would result in a hopelessly complex model to perform analytical calculations. Here, we propose to use a modified Mori-Tanaka approach to better predict the elastic properties of the nanocomposite. Hence, in the Mori-Tanaka formulas we assume that we may have particles of different thicknesses depending on the reinforcement percentage. That is for each percentage, we assume a composition with different particle thicknesses. As a consequence, at high percentages larger N values and at lower percentages smaller N values were used in the calculations. However, for epoxy based specimens N=6 was assumed.

Table 2. shows the composition of nanoclay particles depending on the reinforcement percentage.

Table 2. Nanoclay flake number composition for each percentage

Nanoclay Reinforcement	Composition of Flakes Number
0.2%	100% N=1
1%	40% N=1 30% N=2 30% N=3
3%	40% N=2 30% N=3 30% N=4
6%	100% N=5
10%	100% N=6

Using this composition, we recalculated the Mori-Tanaka results for three different formulations namely, "Oriented Particles", "2-D randomly distributed particles" and "3-D randomly distributed particles" to account for possible different nanoclay particle distribution. In all the calculations, the particle diameter D was kept constant.

Matrix1 : PP 3371

E_m = average experimental Young's modulus at each temperature

ν_m = average experimental Poisson's ratio result at each temperature

V_m = volume fraction of matrix (calculated from weight fraction of matrix)

W_m = weight fraction of matrix

γ_m = 8,829N/m^3 (specific weight of matrix)

μ_m = calculated average experimental shear modulus at each temperature

λ_m = calculated average experimental Lamé constant at each temperature

Matrix 2: EPON 828 epoxy

E_m = 2.8177 GPa (average experimental result at room temperature)

ν_m = 0. 3105 (average experimental result at room temperature)

V_m = volume fraction of matrix (calculated from weight fraction of matrix)

W_m = weight fraction of matrix

γ_m = 15,696N/m^3 (specific weight of matrix)

μ_m = 1.075 GPa (calculated)

λ_m = 1.762 GPa (calculated)

Particle : Nanoclay

$E_{nanoclay}$ = 300 GPa (assumed from molecular dynamics calculations)

E_p = effective Young's modulus of particle = $E_{nanoclay}(N.d_s/t)$ (Referring to [2] and Figure 1)

ν_p = 0. 2 (assumed)

$V_p = c$ = volume fraction of nanoclay (calculated from weight fraction of nanoclay)

W_p = weight fraction of nanoclay

γ_p = 18,639 N/m^3 (specific weight of nanoclay)

μ_p = effective shear modulus calculated for each particle geometry

λ_p = effective Lamé constant calculated for each particle geometry

The average experimental values of the Young's modulus (E_m) and Poisson's ratio (ν_m) for PP 3371 at each temperature are summarized in Table 3.

Table 3. Elastic properties of PP 3371 at various temperatures

Temperature	Young's Modulus E_m (GPa)	Poisson's Ratio
-65°F	3.866	0.3429
-4°F	3.346	0.3438
RT	1.200	0.3947
120°F	0.616	0.4038
-160°F	0.392	0.4256

2.1-1) Oriented Nanoclay Particles

Referring to [15], the normalized longitudinal Young's modulus (parallel to the tensile test direction), the normalized transverse Young's modulus, the normalized in plane shear modulus, the normalized out of plane shear modulus, the normalized plane strain bulk modulus and the major Poisson's ratio can be expresses as:

$$\frac{E_{11}}{E_m} = \frac{1}{1 + c\left[-2\nu_m A_3 + (1-\nu_m)A_4 + (1+\nu_m)A_5 A\right]/2A} \tag{3}$$

$$\frac{E_{22}}{E_m} = \frac{1}{1 + c(A_1 + 2\nu_m A_2)A} \tag{4}$$

$$\frac{\mu_{21}}{\mu_m} = 1 + \frac{c}{\frac{\mu_m}{\mu_p - \mu_m} + 2(1-c)S_{1212}} \tag{5}$$

$$\frac{\mu_{13}}{\mu_0} = 1 + \frac{c}{\frac{\mu_m}{\mu_p - \mu_m} + 2(1-c)S_{2323}} \tag{6}$$

$$\frac{K_{13}}{K_m} = \frac{(1+\nu_m)(1-2\nu_m)}{1-\nu_m(1+2\nu_{21}) + c\left\{2(\nu_{21}-\nu_m)A_3 + \left[1-\nu_m(1+2\nu_{21})\right]A_4\right\}/A} \tag{7}$$

where $K_m = \lambda_m + \mu_m$

$$\nu_{21}^2 = \frac{E_{22}}{E_{11}} - \frac{E_{22}}{4}\left(\frac{1}{\mu_{13}} + \frac{1}{K_{13}}\right) \tag{8}$$

and c is the volume fraction of nanoclay and the coefficients A_1, A_2, A_3, A_4, A_5 and a are given by:

$$A_1 = D_1\left(B_4 + B_5\right) - 2B_2 \tag{9}$$

$$A_2 = \left(1 + D_1\right)B_2 - \left(B_4 + B_5\right) \tag{10}$$

$$A_3 = B_1 - D_1 B_3 \tag{11}$$

$$A_4 = \left(1 + D_1\right) B_1 - 2B_3 \tag{12}$$

$$A_5 = \left(1 - D_1\right) / \left(B_4 - B_5\right) \tag{13}$$

and

$$A = 2B_2 B_3 - B_1 \left(B_4 + B_5\right) \tag{14}$$

with

$$B_1 = cD_1 + D_2 + \left(1 - c\right)\left(D_1 S_{1111} + 2S_{2211}\right) \tag{15}$$

$$B_2 = c + D_3 + \left(1 - c\right)\left(D_1 S_{1122} + S_{2222} + S_{2233}\right) \tag{16}$$

$$B_3 = c + D_3 + \left(1 - c\right)\left[S_{1111} + \left(1 + D_1\right) S_{2211}\right] \tag{17}$$

$$B_4 = cD_1 + D_2 + \left(1 - c\right)\left(S_{1122} + D_1 S_{2222} + S_{2233}\right) \tag{18}$$

$$B_5 = c + D_3 + \left(1 - c\right)\left(S_{1122} + S_{2222} + D_1 S_{2233}\right) \tag{19}$$

and

$$D_1 = 1 + 2\left(\mu_p - \mu_m\right) \Big/ \left(\lambda_p - \lambda_m\right) \tag{20}$$

$$D_2 = \left(\lambda_m + 2\mu_m\right) \Big/ \left(\lambda_p - \lambda_m\right) \tag{21}$$

$$D_3 = \lambda_m \Big/ \left(\lambda_p - \lambda_m\right) \tag{22}$$

The D_i (i=1,2,3) terms are defined by using μ_m, λ_m and μ_p, λ_p, which are the Lame constants of the matrix and particles, respectively. In the B_i (i=1,2,3) terms, the components of Eshelby's tensor S_{ijkl} given below are used:

$$S_{1111} = \frac{1}{2\left(1 - \nu_m\right)} \left\{ 1 - 2\nu_m + \frac{3\alpha^2 - 1}{\alpha^2 - 1} - \left[1 - 2\nu_m + \frac{3\alpha^2}{\alpha^2 - 1} \right] g \right\} \tag{22}$$

$$S_{2222} = S_{3333} = \frac{3}{8(1-\nu_m)}\frac{\alpha^2}{\alpha^2-1} + \frac{1}{4(1-\nu_m)}\left[1-2\nu_m - \frac{9}{4(\alpha^2-1)}\right]g \tag{23}$$

$$S_{2233} = S_{3322} = \frac{1}{4(1-\nu_m)}\left\{\frac{\alpha^2}{2(\alpha^2-1)} - \left[1-2\nu_m + \frac{3}{4(\alpha^2-1)}\right]g\right\} \tag{24}$$

$$S_{2211} = S_{3311} = -\frac{1}{2(1-\nu_m)}\frac{\alpha^2}{\alpha^2-1} + \frac{1}{4(1-\nu_m)}\left\{\frac{3\alpha^2}{\alpha^2-1} - (1-2\nu_m)\right\}g \tag{25}$$

$$S_{1122} = S_{1133} = -\frac{1}{2(1-\nu_m)}\left[1-2\nu_m + \frac{1}{\alpha^2-1}\right] + \frac{1}{2(1-\nu_m)}\left[1-2\nu_m + \frac{3}{2(\alpha^2-1)}\right]g \tag{26}$$

$$S_{2323} = S_{3232} = \frac{1}{4(1-\nu_m)}\left\{\frac{\alpha^2}{2(\alpha^2-1)} + \left[1-2\nu_m - \frac{3}{4(\alpha^2-1)}\right]g\right\} \tag{27}$$

$$S_{1212} = S_{1313} = \frac{1}{4(1-\nu_m)}\left\{1-2\nu_m - \frac{\alpha^2+1}{\alpha^2-1} - \frac{1}{2}\left[1-2\nu_m - \frac{3(\alpha^2+1)}{\alpha^2-1}\right]g\right\} \tag{28}$$

Here ν_m is the Poisson's ratio of the matrix. In Eshelby's tensor, the g term has two different expressions depending on the aspect ratio of the inclusion:

$$g' = \frac{\alpha}{(\alpha^2-1)^{3/2}}\left\{\alpha(\alpha^2-1)^{1/2} - \cosh^{-1}\alpha\right\} \quad \text{when } \alpha > 1 \tag{29.a}$$

$$g = \frac{\alpha}{(1-\alpha^2)^{3/2}}\left\{\cos^{-1}\alpha - \alpha(1-\alpha^2)^{1/2}\right\} \quad \text{when } \alpha < 1 \tag{29.b}$$

Using the particle composition assumed in Table 2, the Young's modulus and Poisson's ratio are calculated for each reinforcement percentage at each temperature. The results are summarized in Tables 4 and 5 for PP 3371 and epoxy respectively and compared with the experimental data presented in [1].

Table 4. Comparison of Mori-Tanaka and Experimental results for oriented particles in PP 3371 matrix (D_p=200 nm, $E_{nanoclay}$=300 GPa) at each temperature

PP 3371 Reinforcement	$E_{nanoclay}$ (GPa)	D_p (nm)	Particle Composition	E_p (GPa)	t_p (nm)	Temperature	Young's M. (Exp.) (GPa)	E_{11} (GPa)	Poisson's Ratio (Exp.)	ν_{12}
0.2%	300	200	100% N=1	300	0.615	-65°F	4.284	4.078	0.3283	0.3467
						-4°F	3.713	3.5514	0.3307	0.3481
						RT	1.317	1.3379	0.4167	0.4072
						120°F	0.728	0.7079	0.4350	0.4212
						160°F	0.449	0.4586	0.4782	0.4481
1%	300	200	40% N=1 30% N=2 30% N=3	300 122.388 102.216	0.615 3.015 5.415	-65°F	4.603	4.46795	0.3193	0.35255
						-4°F	4.008	3.92262	0.3156	0.35453
						RT	1.508	1.56593	0.4056	0.4216
						120°F	0.765	0.85319	0.4631	0.43839
						160°F	0.465	0.56118	0.4715	0.46875
3%	300	200	40% N=2 30% N=3 30% N=4	122.388 102.216 94.434	3.015 5.415 7.815	-65°F	4.694	4.68366	0.3076	0.35622
						-4°F	4.179	4.11276	0.3114	0.35843
						RT	1.628	1.61512	0.3852	0.4268
						120°F	0.828	0.86217	0.4355	0.44271
						160°F	0.497	0.55982	0.4523	0.47241
6%	300	200	100% N=5	90.308	10.215	-65°F	4.973	4.8933	0.3039	0.3595
						-4°F	4.212	4.289	0.3056	0.3618
						RT	1.646	1.6472	0.3722	0.4291
						120°F	0.833	0.8664	0.4334	0.4435
						160°F	0.503	0.5583	0.5077	0.4722
10%	300	200	100% N=6	87.753	12.615	-65°F	5.092	5.4202	0.2983	0.3657
						-4°F	4.333	4.765	0.2928	0.3683
						RT	1.742	1.8547	0.3725	0.4397
						120°F	0.866	0.9789	0.4111	0.4551
						160°F	0.515	0.632	0.4896	0.4854

Table 5. Comparison of Mori-Tanaka and Experimental results for oriented particles in epoxy matrix (D_p=200 nm, $E_{nanoclay}$=300 GPa) at RT

PP 3371 Reinforcement	$E_{nanoclay}$ (GPa)	D (nm)	Particle Composition	E_p (GPa)	t_p (nm)	Temperature	Young's M. (Exp.) (GPa)	E_{11} (GPa)	Poisson's Ratio (Exp.)	ν_{12}
0%	300	200	100% N=6	87.753	12.615	RT	2.8177	2.8177	0.3105	0.3105
1%							2.9127	2.8791	0.3238	0.3150
3%							2.9840	2.9977	0.3288	0.3236
6%							3.0965	3.1682	0.3340	0.3316
10%							3.3427	3.3880	0.3348	0.3404

2.1-2) 2-D Randomly Distributed Nanoclay Particles

Here the nanoclay flakes are in a plane parallel to test the direction, but are randomly distributed in the plane. Referring to [16], the normalized in plane Young's modulus, the normalized in plane shear modulus, the normalized out of plane shear modulus and the normalized out of plane Young's modulus for the case of 2-D randomly distributed nanoclay particles can be expressed as:

$$\frac{E_{11}}{E_m} = \left(\frac{1}{1 + cp_{11}} \right) \tag{30}$$

where c is the volume fraction given in equation (2) and p_{11} is:

$$\begin{aligned} p_{11} = {} & \frac{1}{1 + c(b_1 - b_2)} \left\{ \frac{2(a_1 + a_2 - a_3) + a_4 + a_5 a}{16a} - \frac{1}{4\left[2S_{1212} + \mu_m / (\mu_p - \mu_m) \right]} \right\} \\ & - \frac{(1 - \nu_m)(1 + cb_5) + 2c\nu_m b_3}{2c^2 b_3 b_4 - (1 + cb_5)\left[1 + c(b_1 + b_2) \right]} \frac{2(a_1 - a_2 + a_3) + a_4 + a_5 a}{8a} \\ & + \frac{(1 - \nu_m) cb_4 + \nu_m \left[1 + c(b_1 + b_2) \right]}{2c^2 b_3 b_4 - (1 + cb_5)\left[1 + c(b_1 + b_2) \right]} \frac{-2a_2 + a_4 - a_5 a}{4a} \end{aligned} \tag{31}$$

$$\frac{\mu_{12}}{\mu_m} = \left(\frac{1}{1 + cp_{12}} \right) \tag{32}$$

with p_{12} given as:

$$\begin{aligned} p_{12} = {} & \left[2(a_1 + a_2 - a_3) + a_4 + a_5 a - \frac{4a}{2S_{1212} + \mu_m / (\mu_p - \mu_m)} \right] / \\ & \{ 8a + c[(S_{1122} - S_{2222} + 1)(2a_3 - a_4 - a_5 a) \\ & + 2(S_{1111} - S_{2211} - 1)(a_1 + a_2) + (S_{1122} - S_{2233})(2a_3 - a_4 + a_5 a) \\ & - \frac{4a(2S_{1212} - 1)}{2S_{1212} + \mu_m / (\mu_p - \mu_m)}] \} \end{aligned} \tag{33}$$

$$\frac{\mu_{13}}{\mu_m} = \left(\frac{1}{1 + cp_{13}} \right) \tag{34}$$

with p_{13}

$$p_{13} = -\left[\frac{1}{2S_{1313} + \mu_m/(\mu_p - \mu_m)} + \frac{1}{2S_{2323} + \mu_m/(\mu_p - \mu_m)}\right] / \left\{2 - c\left[\frac{2S_{1313} - 1}{2S_{1313} + \mu_m/(\mu_p - \mu_m)} + \frac{2S_{2323} - 1}{2S_{2323} + \mu_m/(\mu_p - \mu_m)}\right]\right\} \tag{35}$$

$$\frac{E_{33}}{E_m} = \frac{1}{1 + cp_{33}} \tag{36}$$

where p_{33} is,

$$p_3 = \left\{\left[\nu_m(1 + cb_5) + cb_3\right](2a_3 + a_4 - a_5 a) - \left[1 + c(b_1 + b_2 + 2\nu_0 b_4)\right](a_4 + a_5 a)\right\} / 2a\left\{2c^2 b_3 b_4 - (1 + cb_5)\left[1 + c(b_1 + b_2)\right]\right\} \tag{37}$$

The definition of the components of Eshelby's tensor and g were given in section 2.1-1. The other constants which are used to calculate the material properties of 2-D randomly distributed nanoclay particles are given below:

$$a_1 = 6(\kappa_p - \kappa_m)(\mu_p - \mu_m)(S_{2222} + S_{2233} - 1) - 2(\kappa_m \mu_p - \kappa_p \mu_m) + 6\kappa_p(\mu_p - \mu_m) \tag{38}$$

$$a_2 = 6(\kappa_p - \kappa_m)(\mu_p - \mu_m)S_{1133} + 2(\kappa_m \mu_p - \kappa_p \mu_0) \tag{39}$$

$$a_3 = -6(\kappa_p - \kappa_m)(\mu_p - \mu_m)S_{3311} - 2(\kappa_m \mu_p - \kappa_p \mu_m) \tag{40}$$

$$a_4 = 6(\kappa_p - \kappa_m)(\mu_p - \mu_m)(S_{1111} - 1) + 2(\kappa_m \mu_p - \kappa_p \mu_m) + 6\mu_p(\kappa_p - \kappa_m) \tag{41}$$

$$a_5 = 1/[S_{3322} - S_{3333} + 1 - \mu_p/(\mu_p - \mu_m)] \tag{42}$$

$$\begin{aligned} a = {} & 6(\kappa_p - \kappa_m)(\mu_p - \mu_m)[2S_{1133}S_{3311} - (S_{1111} - 1)(S_{3322} + S_{3333} - 1)] \\ & + 2(\kappa_m \mu_p - \kappa_p \mu_m)[2(S_{1133} + S_{3311}) + (S_{1111} - S_{3322} - S_{3333})] \\ & - 6\kappa_p(\mu_p - \mu_m)(S_{1111} - 1) - 6\mu_p(\kappa_p - \kappa_m)(S_{2222} + S_{2233} - 1) - 6\kappa_p \mu_p \end{aligned} \tag{43}$$

$$b_1 = (1/16a)\{2a_3(6S_{1122} + S_{2222} + S_{2233} - 1) + a_4[3(S_{2222} + S_{2233} - 1) + 2S_{1122}] + 3a_5 a(S_{2222} - S_{2233} - 1) + 2a_1[3(S_{1111} - 1) + S_{2211}] - 2a_2(S_{1111} + 3S_{2211} - 1) - 4a(2S_{1212} - 1)/[2S_{1212} + \mu_m/(\mu_p - \mu_m)]\} \quad (44)$$

$$b_2 = (1/16a)\{2a_3\left[2S_{1111} + 3(S_{2222} + S_{2233} - 1)\right] + a_4(6S_{1122} + S_{2222} + S_{2233} - 1) + a_5 a(S_{2222} - S_{2233} - 1) + 2a_1(S_{1111} + 3S_{2211} - 1) - 2a_2\left[S_{2211} + 3(S_{1111} - 1)\right] + 4a(2S_{1212} - 1)/\left[2S_{1212} + \mu_m/(\mu_p - \mu_m)\right]\} \quad (45)$$

$$b_3 = (1/a)\{-2a_2(S_{1111} + S_{2211} - 1) + a_4(2S_{1122} + S_{2222} + S_{2233} - 1) - a_5 a(S_{2222} - S_{2233} - 1)\} \quad (46)$$

$$b_4 = (1/4a)\{2(a_1 - a_2)S_{2211} + (2a_3 + a_4)(S_{2222} + S_{2233} - 1) - a_5 a(S_{2222} - S_{2233} - 1)\} \quad (47)$$

$$b_5 = (1/2a)\{-2a_2 S_{2211} + a_4(S_{2222} + S_{2233} - 1) + a_5 a(S_{2222} - S_{2233} - 1)\} \quad (48)$$

Again using the particle composition given in Table 2, the elastic properties are calculated for each reinforcement percentage and at each temperature. The calculated results for 2-D randomly distributed particles for PP 3371 and epoxy are summarized in Tables 6. and 7. respectively and compared with those obtained experimentally [1].

Table 6. Comparison of Mori-Tanaka and Experimental results for 2-D randomly distributed particles in PP 3371 matrix (D_p=200 nm, $E_{nanoclay}$=300 GPa) at each temperature

PP 3371 Reinforcement	$E_{nanoclay}$ (GPa)	D (nm)	Particle Composition	E_p (GPa)	t_p (nm)	Temperature	Young's M. (Exp.) (GPa)	E_{11} (GPa)	Poisson's Ratio (Exp.)	ν_{12}
0.2%	300	200	100% N=1	300	0.615	-65°F	4.284	3.9547	0.3283	0.348
						-4°F	3.713	3.4325	0.3307	0.3495
						RT	1.317	1.2607	0.4167	0.4086
						120°F	0.728	0.6565	0.4350	0.4225
						160°F	0.449	0.4222	0.4782	0.4493
1%	300	200	40% N=1 30% N=2 30% N=3	300 122.388 102.216	0.615 3.015 5.415	-65°F	4.603	4.11997	0.3193	0.35506
						-4°F	4.008	3.58864	0.3156	0.35711
						RT	1.508	1.35765	0.4056	0.42201
						120°F	0.765	0.71777	0.4631	0.43709
						160°F	0.465	0.4664	0.4715	0.46639
3%	300	200	40% N=2 30% N=3 30% N=4	122.388 102.216 94.434	3.015 5.415 7.815	-65°F	4.694	4.23049	0.3076	0.35911
						-4°F	4.179	3.68571	0.3114	0.36125
						RT	1.628	1.38646	0.3852	0.42721
						120°F	0.828	0.72621	0.4355	0.44188
						160°F	0.497	0.46902	0.4523	0.47103
6%	300	200	100% N=5	90.308	10.215	-65°F	4.973	4.3515	0.3039	0.3619
						-4°F	4.212	3.7884	0.3056	0.3639
						RT	1.646	1.4118	0.3722	0.4286
						120°F	0.833	0.7343	0.4334	0.4422
						160°F	0.503	0.4724	0.5077	0.4706
10%	300	200	100% N=6	87.753	12.615	-65°F	5.092	4.6144	0.2983	0.3676
						-4°F	4.333	4.0236	0.2928	0.3699
						RT	1.742	1.5141	0.3725	0.4369
						120°F	0.866	0.7895	0.4111	0.451
						160°F	0.515	0.5092	0.4896	0.4809

Table 7. Comparison of Mori-Tanaka and Experimental results for 2-D randomly distributed particles in epoxy matrix (D_p=200 nm, $E_{nanoclay}$=300 GPa) at RT

PP 3371 Reinforcement	$E_{nanoclay}$ (GPa)	D (nm)	Particle Composition	E_p (GPa)	t_p (nm)	Temperature	Young's M. (Exp.) (GPa)	E_{11} (GPa)	Poisson's Ratio (Exp.)	ν_{12}
0%	300	200	100% N=6	87.753	12.615	RT	2.8177	2.8177	0.3105	0.3105
1%							2.9127	3.0249	0.3238	0.3119
3%							2.9840	3.4486	0.3288	0.3399
6%							3.0965	4.1083	0.3340	0.4168
10%							3.3427	5.0367	0.3348	0.5236

2.1-3) 3-D Randomly Distributed Nanoclay Particles

Again referring to [16], the effective bulk modulus, shear modulus, Young's modulus and Poisson's ratio for the case of 3-D randomly distributed particles can be expressed as:

$$p = \frac{p_2}{p_1} \tag{49}$$

$$q = \frac{q_2}{q_1} \tag{50}$$

$$p_1 = 1 + c\frac{\left[2\left(S_{1122} + S_{2222} + S_{2233} - 1\right)\left(a_3 + a_4\right) + \left(S_{1111} + 2S_{2211} - 1\right)\left(a_1 - 2a_2\right)\right]}{3a} \tag{51}$$

$$p_2 = \frac{\left[a_1 - 2\left(a_2 - a_3 - a_4\right)\right]}{3a} \tag{52}$$

$$\begin{aligned} q_1 = 1 - c\Bigg\{ & \frac{2}{5}\frac{2S_{1212} - 1}{2S_{1212} + \dfrac{\mu_0}{\left(\mu_1 - \mu_0\right)}} + \frac{1}{3}\frac{2S_{2323} - 1}{2S_{2323} + \dfrac{\mu_0}{\left(\mu_1 - \mu_0\right)}} - \frac{1}{15a}\Big[\left(S_{1122} - S_{2233}\right)\left(2a_3 - a_4 + a_5 a\right) \\ & + 2\left(S_{1111} - S_{2211} - 1\right)\left(a_1 + a_2\right) + \left(S_{1122} - S_{2222} + 1\right)\left(2a_3 - a_4 - a_5 a\right)\Big]\Bigg\} \end{aligned} \tag{53}$$

$$\begin{aligned} q_2 = & -\frac{2}{5}\frac{1}{2S_{1212} + \dfrac{\mu_m}{\left(\mu_p - \mu_m\right)}} - \frac{1}{3}\frac{1}{2S_{2323} + \dfrac{\mu_m}{\left(\mu_p - \mu_m\right)}} \\ & + \frac{1}{15a}\left[2\left(a_1 + a_2 - a_3\right) + a_4 + a_5 a\right] \end{aligned} \tag{54}$$

$$\kappa = \frac{\kappa_m}{1 + cp} \tag{55}$$

$$\mu = \frac{\mu_m}{1+cp} \tag{56}$$

$$E = \frac{3\mu}{1+\frac{\mu}{3\kappa}} \tag{57}$$

$$\nu = \frac{1}{2} - \frac{E}{6\kappa} \tag{58}$$

All the constant coefficients appearing in Eqs. (49-58) were given in sections 2.1-1 and 2.1-2

Using the above formulation, the Young's modulus and Poisson's ratio are computed for PP 3371 and epoxy and displayed in Tables 8 and 9 respectively. For comparison purpose the experimental results presented in [1] for each reinforcement percentage and at each temperature are also included in Tables 8 and 9.

Table 8. Comparison of Mori-Tanaka and Experimental results for 3-D randomly distributed particles in PP 3371 matrix (D_p=200 nm, $E_{nanoclay}$=300 GPa) at each temperature

PP 3371 Reinforcement	$E_{nanoclay}$ (GPa)	D (nm)	Particle Composition	E_p (GPa)	t_p (nm)	Temperature	Young's M. (Exp.) (GPa)	E_{11} (GPa)	Poisson's Ratio (Exp.)	ν_{12}
0.2%	300	200	100% N=1	300	0.615	-65°F	4.284	3.9772	0.3283	0.3406
						-4°F	3.713	3.4543	0.3307	0.3412
						RT	1.317	1.2741	0.4167	0.3903
						120°F	0.728	0.6656	0.4350	0.3983
						160°F	0.449	0.4284	0.4782	0.4203
1%	300	200	40% N=1 30% N=2 30% N=3	300 122.388 102.216	0.615 3.015 5.415	-65°F	4.603	4.18724	0.3193	0.33662
						-4°F	4.008	3.65366	0.3156	0.33689
						RT	1.508	1.39857	0.4056	0.3837
						120°F	0.765	0.74513	0.4631	0.39066
						160°F	0.465	0.48553	0.4715	0.41289
3%	300	200	40% N=2 30% N=3 30% N=4	122.388 102.216 94.434	3.015 5.415 7.815	-65°F	4.694	4.31937	0.3076	0.33434
						-4°F	4.179	3.77001	0.3114	0.33461
						RT	1.628	1.43102	0.3852	0.38224
						120°F	0.828	0.75303	0.4355	0.39015
						160°F	0.497	0.48657	0.4523	0.413
6%	300	200	100% N=5	90.308	10.215	-65°F	4.973	4.4607	0.3039	0.3325
						-4°F	4.212	3.8898	0.3056	0.3329
						RT	1.646	1.4581	0.3722	0.3818
						120°F	0.833	0.7603	0.4334	0.3904
						160°F	0.503	0.4889	0.5077	0.4136
10%	300	200	100% N=6	87.753	12.615	-65°F	5.092	4.7831	0.2983	0.3279
						-4°F	4.333	4.1795	0.2928	0.3282
						RT	1.742	1.5842	0.3725	0.3767
						120°F	0.866	0.8285	0.4111	0.3854
						160°F	0.515	0.534	0.4896	0.4091

Table 9. Comparison of Mori-Tanaka and Experimental results for 3-D randomly distributed particles in epoxy matrix (D_p=200 nm, $E_{nanoclay}$=300 GPa) at RT

PP 3371 Reinforcement	$E_{nanoclay}$ (GPa)	D (nm)	Particle Composition	E_p (GPa)	t_p (nm)	Temperature	Young's M. (Exp.) (GPa)	E_{11} (GPa)	Poisson's Ratio (Exp.)	ν_{12}
0%	300	200	100% N=6	87.753	12.615	RT	2.8177	2.8177	0.3105	0.3105
1%							2.9127	2.9363	0.3238	0.3077
3%							2.9840	3.1794	0.3288	0.3025
6%							3.0965	3.5594	0.3340	0.2953
10%							3.3427	4.0978	0.3348	0.2868

2.1-4) Comparison of Experimental Results with Mori-Tanaka Calculations for PP Based Nanocomposites

To compare the experimental results with those predicted using the modified Mori-Tanaka formulations, we first display their variation with temperature for each reinforcement percentage. Figures 2.(a)-(e) depict the comparison of the three Mori-Tanaka calculations (for oriented, 2-D randomly distributed and 3-D randomly distributed particles) with the experimental results.

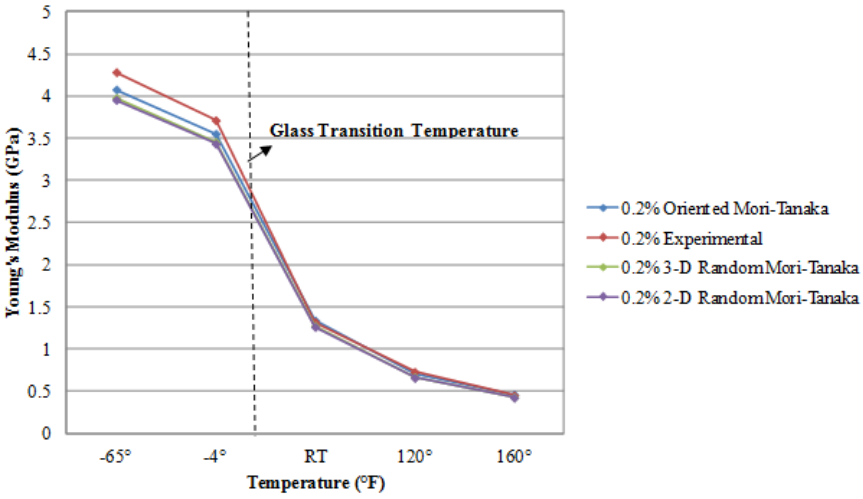

(a)

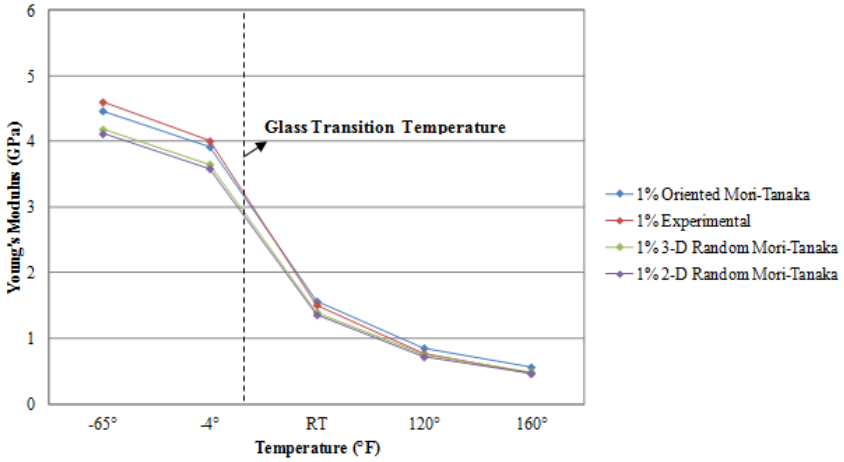

(b)

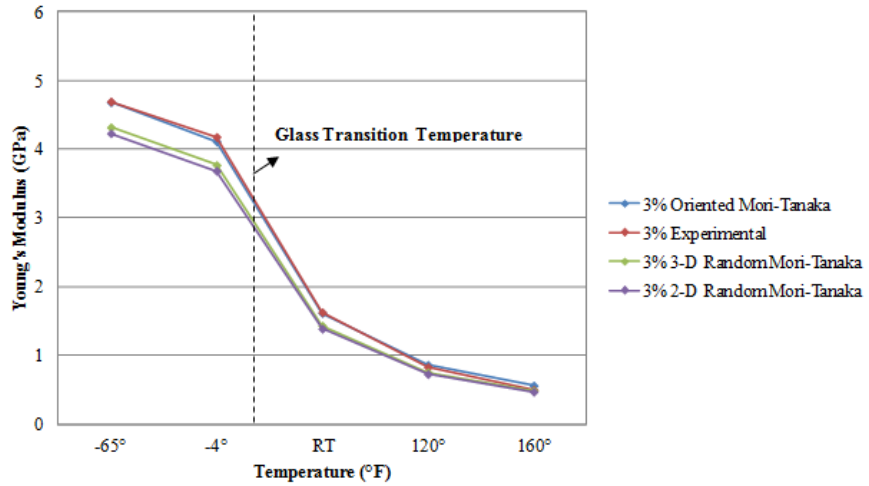

(c)

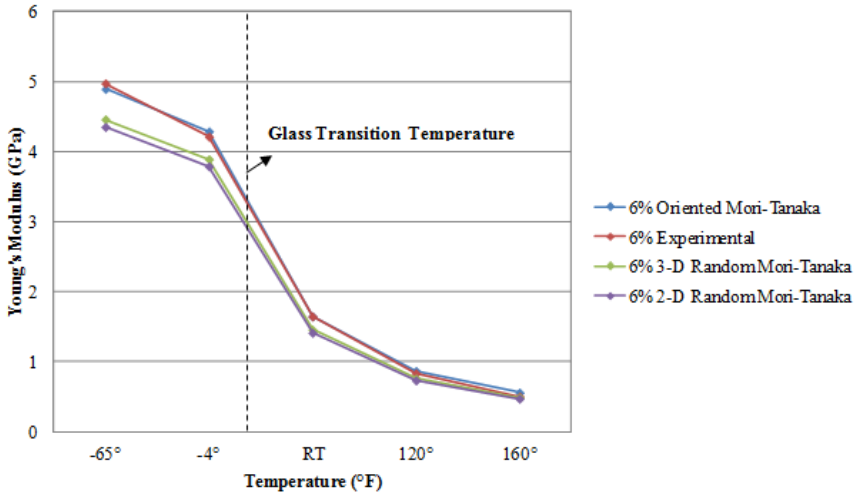

(d)

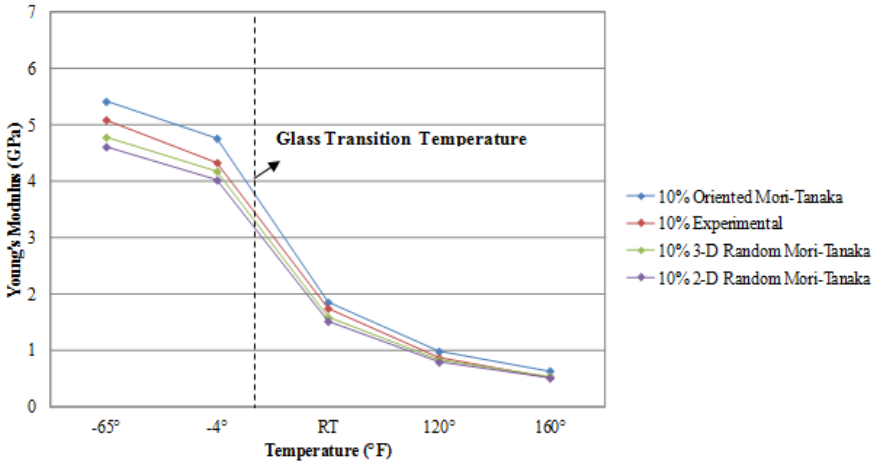

(e)

Figure 2. Comparison of Young's modulus obtained from Mori-Tanaka formulations and experimental results of nanoclay reinforced PP 3371 specimens at various temperatures (a) for 0.2%, (b) for 1%, (c) for 3%, (d) for 6% and (e) for 10%

The results shown above first indicate that the Mori-Tanaka calculations compare well with those obtained experimentally. The results for oriented particles appear to provide the best fit with the experimental data for all reinforcement percentages. The results for 2-D and 3-D randomly distributed particles appear to be close to each other. As was discussed in [1], the Young's modulus drops significantly when the temperature increases from -4°F to room temperature. This is due to the fact that the glass transition temperature T_g of PP is around 14°F and the material goes from a glassy state to a rubbery state. The Mori-Tanaka calculations also capture this feature. Since the Young's modulus results at lower temperatures are approximately one order of magnitude higher than those at higher temperatures, it is difficult to discern from Figure 2. the relative effect of temperature on the best fit with experimental data. Thus the variation of the Young's modulus with reinforcement percentage is plotted for each temperature and displayed in Fig 3 (a)-(e).

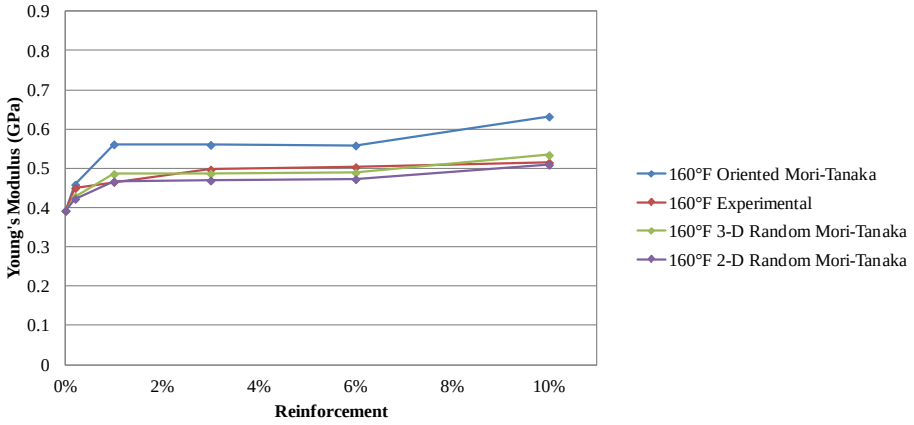

(a)

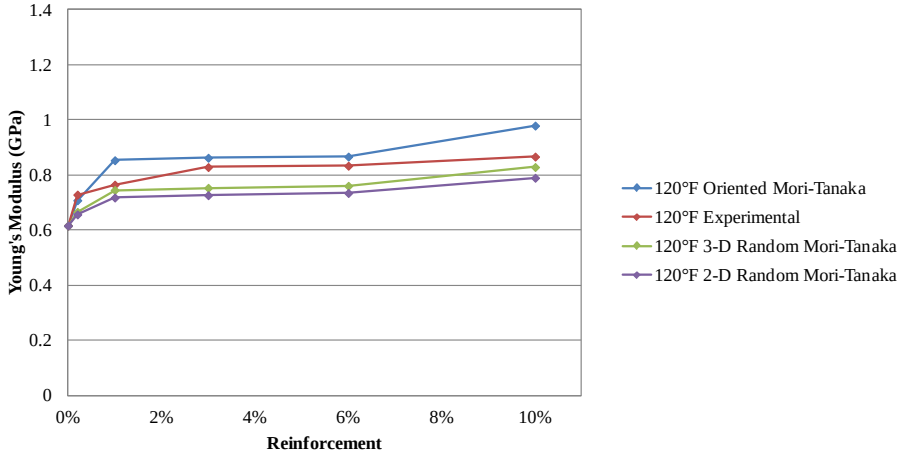

(b)

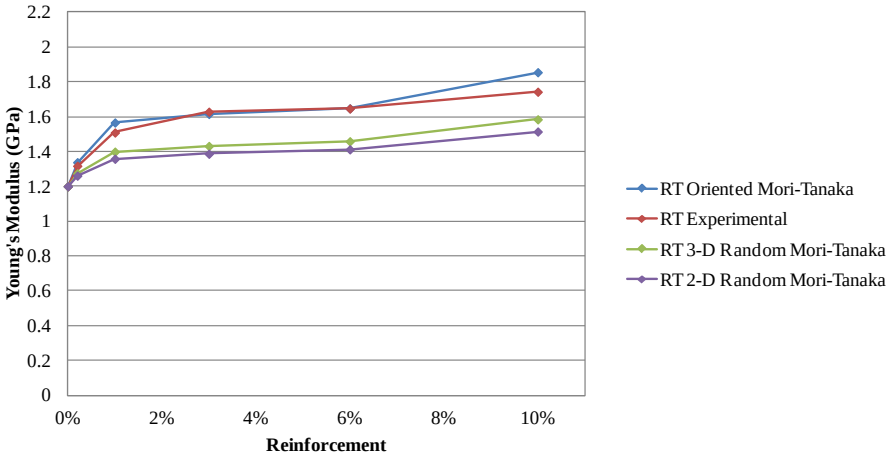

(c)

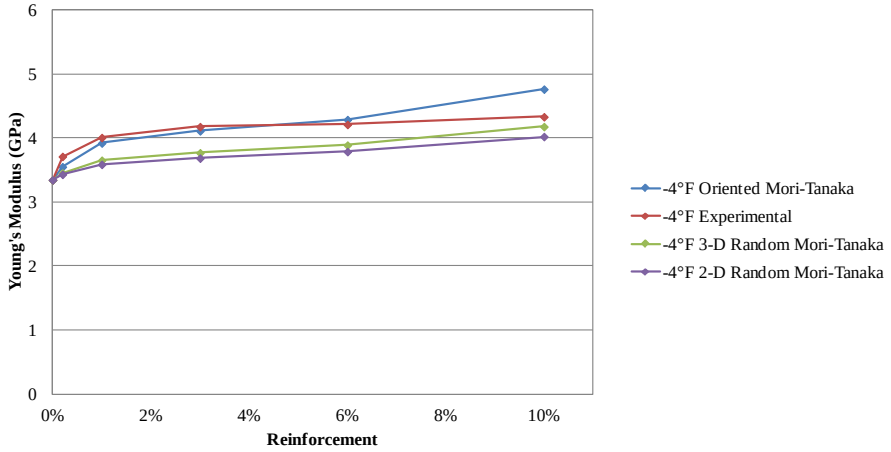

(d)

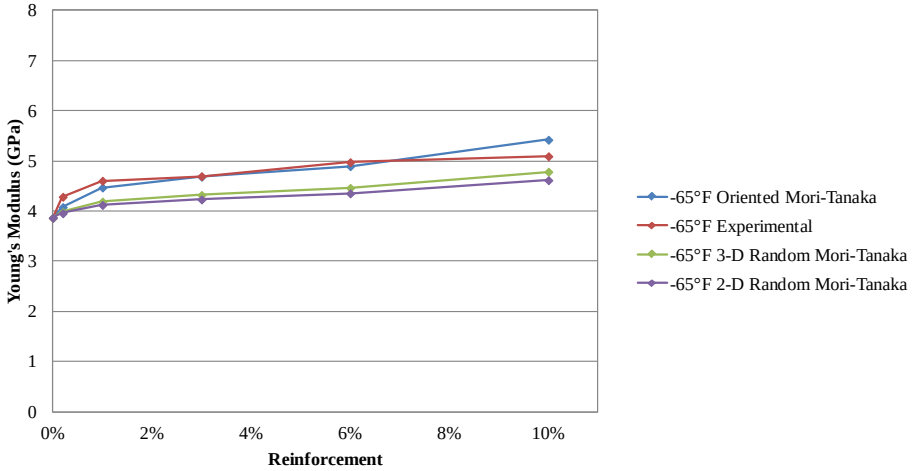

(e)

Figure 3. Comparison of Young's modulus obtained from experimental and from oriented, 2-D and 3-D random Mori-Tanaka calculations for various nanoclay reinforcement percentages (a) at 160°F, (b) at 120°F, (c) at RT, (d) at -4°F and (e) at -65°F

As noted earlier, the Mori-Tanaka results for oriented particles best fit the experimental results, except at 120°F and 160°F. At 160°F the results for 3-D randomly distributed particles are closer to the experimental results. One may also note that at 10% reinforcement there is a significant difference between the predicted Mori-Tanaka and experimental results. This discrepancy at higher reinforcement percentage was also reported in [2]. This may be due to agglomeration of nanoclay particles at higher percentages resulting in larger particle size, and consequently higher Young's modulus.

Extensive results were also obtained for the Poisson's ratio (see [12]). Here we provide sample results and their comparison with experimental data for one reinforcement percentage and one temperature value only. The comparisons are displayed in Figures 4 and 5.

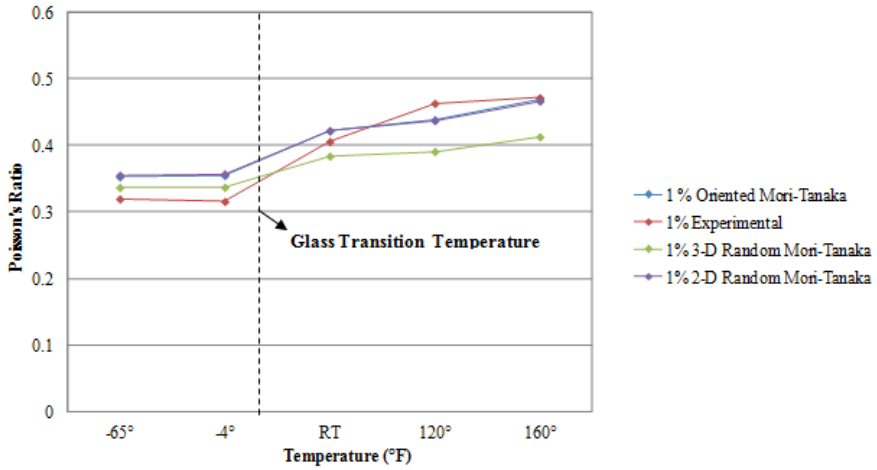

Figure 4. Comparison of Poisson's ratios obtained from Mori-Tanaka formulations and experimental results for 1% nanoclay reinforced PP 3371 specimens at various temperatures

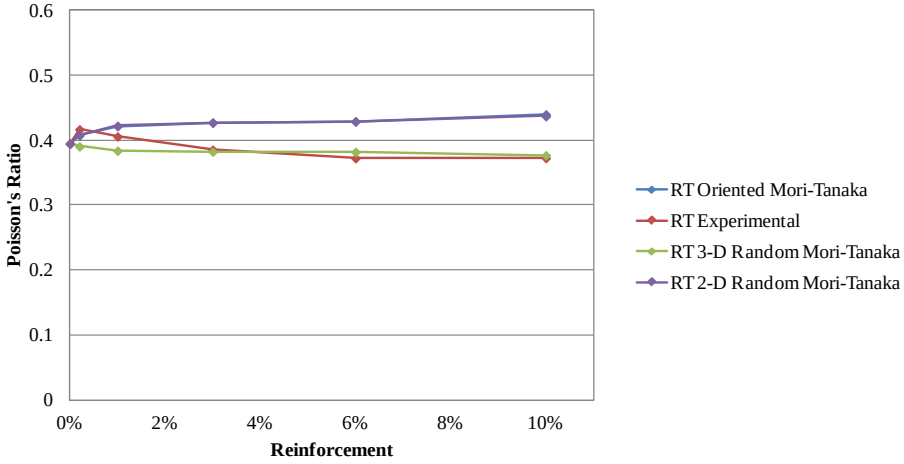

Figure5. Comparison of Poisson's ratios obtained from experiments and oriented, 2-D and 3-D random Mori-Tanaka calculations at RT for various reinforcement percentages

Figure 4. shows the variation of Poisson's ratios obtained from the three Mori-Tanaka formulations with temperature for 1% reinforcement and their comparison with the experimental results. It may be noted that the theoretical predictions by and large match the experimental results both in terms of magnitude and trend. As was noted in [1], some of the difference between theory and experiment may be due to the difficulty in measuring the Poisson's ratio accurately, especially at higher temperatures. It is also observed that, the change in the value of Poisson's ratio is more pronounced around the glass transition temperature. Figure5. depicts the variation of the Poisson's ratio with reinforcement percentage at RT. The results are again compared with the experimental data. In general the theoretical calculations give a reasonable estimate of the Poisson's ratio. For this case (at RT), the results for 3-D randomly distributed particles appear to fit best the experimental data.

2.1-5) Comparison of experimental results with Mori-Tanaka calculations for epoxy based nanocomposites

Figures 6 and 7 show the comparison of Young's modulus and Poisson's ratio obtained from experiments and Mori-Tanaka calculations for EPON 828 epoxy nanoclay reinforced specimens at room temperature. For epoxy there is divergence between experimental and calculated results. This may be due to the fact that more agglomeration of nanoclay particles may occur because of the higher viscosity of epoxy relative to PP.

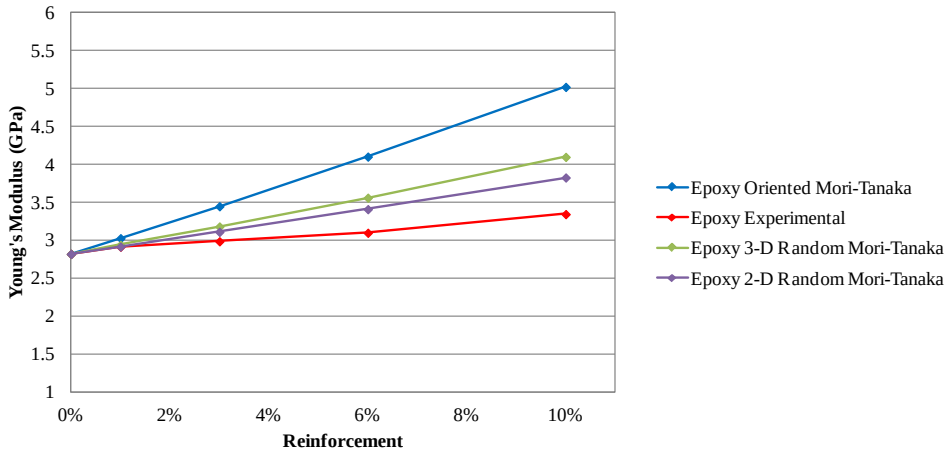

Figure 6. Comparison of Young's modulus obtained from experiments and Mori-Tanaka calculations for oriented, 2-D randomly distributed and 3-D randomly distributed particles at room temperature

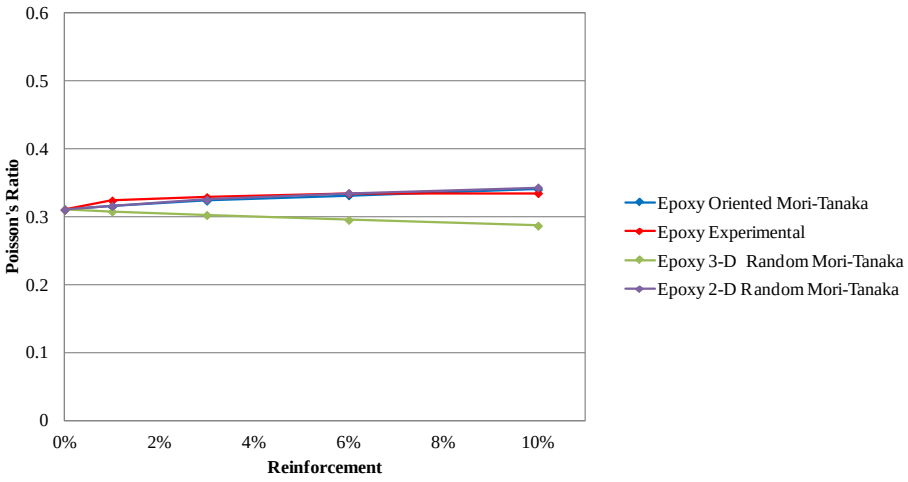

Figure 7. Comparison of Poisson's ratio obtained from experiments and Mori-Tanaka calculations for oriented, 2-D randomly distributed and 3-D randomly distributed particles at room temperature

2.2 EFFECT OF VOIDS

When SEM pictures of the nanocomposite are analyzed, it is observed that at high reinforcement percentages (contrary to low percentages) there may be voids between the particles and matrix. Because of this observation it was decided to modify the Mori-Tanaka calculations by including the effect of voids.

We assume a parabolic distribution of voids as a function of reinforcement percentage since there are fewer voids at lower percentages than at higher percentages. With this assumption the volume fraction of particles can be calculated as follows:

Defining,

V_d : maximum void percentage

W_p: nanoclay weight percentage

ϑ_d: void fraction at each percentage

The parabolic void distribution can be expressed as:

$$\vartheta_d = AW_p{}^2 \tag{59}$$

Assuming maximum void percentage occurs at W_p=10% the unknown A can be obtained from:

$$V_d = A(0.1)^2 \rightarrow A = 100V_d$$

Thus, Eq. (59) becomes:

$$\vartheta_d = 100 V_d {W_p}^2 \quad (60)$$

The total volume V and total weight W are:

$$V = V_p + V_m + V_v \quad (61)$$
$$W_p + W_m = 1 \quad (62)$$

where,

V_p: total volume of particles

V_m: total volume of matrix

V_v: total volume of voids

From,

$$V_p + V_m = \frac{W.W_p}{\gamma_p} + \frac{W(1 - W_p)}{\gamma_m} \quad (63)$$
$$V_v = V\vartheta_d \quad (64)$$

where γ_p and γ_m are the specific weights of nanoclay and matrix respectively. The total volume V is obtained as:

$$V = \frac{W.W_p}{\gamma_p} + \frac{W(1 - W_p)}{\gamma_m} + V\vartheta_d$$

or

$$V = \frac{W.\frac{W_p}{\gamma_p} + W\frac{(1 - W_p)}{\gamma_m}}{(1 - v_d)} \quad (65)$$

With the new total volume V, we redefine the volume fraction c of particles in the presence of voids as:

$$c = \frac{V_p}{V} = \frac{\frac{W_p}{\gamma_p}(1 - \vartheta_d)}{\frac{W_p}{\gamma_p} + \frac{1 - W_p}{\gamma_m}} \quad (66)$$

In the ensuing sections, the Young's modulus and the Poisson's ratio are recalculated using the three different Mori-Tanaka approaches with the new volume fraction c. For all cases the maximum void fraction V_d is assumed to be 6%.

2.2-1) Oriented Nanoclay Particles with Effect of Voids

Figures 8-17 show the comparison of experimental results and oriented Mori-Tanaka calculations with and without voids at various temperatures.

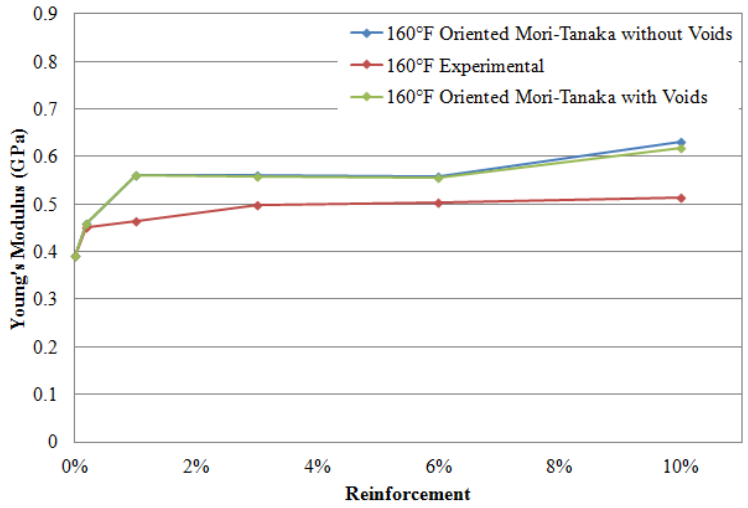

Figure 8. Comparison of Young's modulus obtained from experiments and oriented Mori-Tanaka calculations with and without voids at 160°F

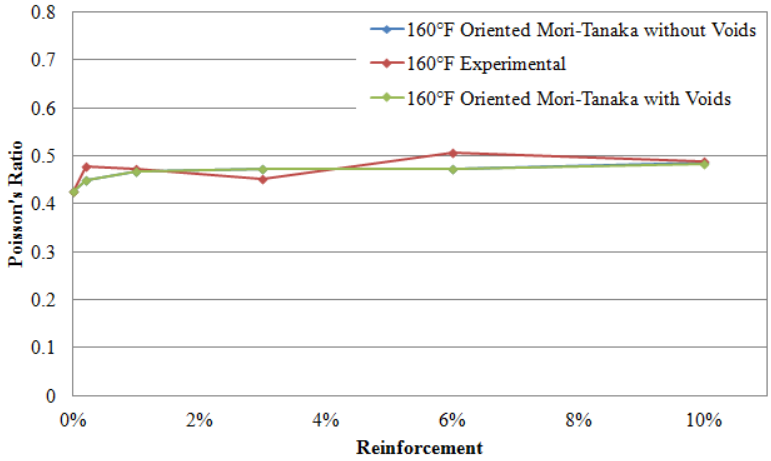

Figure 9. Comparison of Poisson's ratio obtained from experiments and oriented Mori-Tanaka calculations with and without voids at 160°F

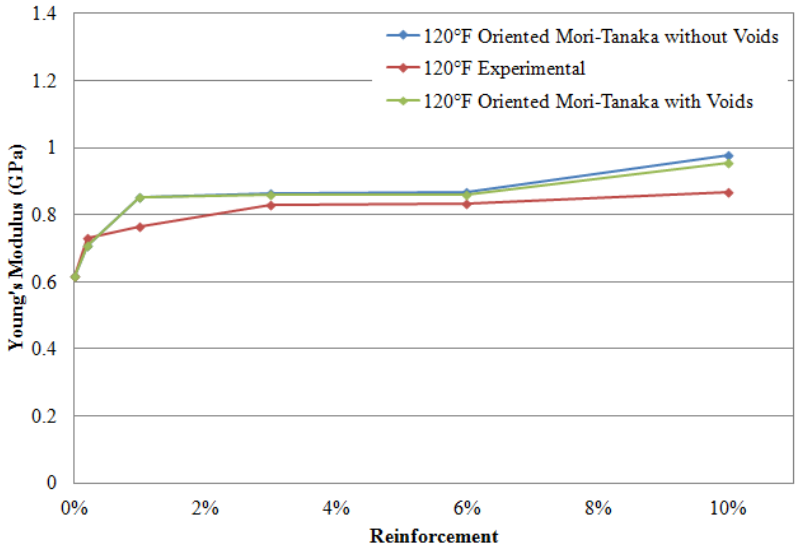

Figure 10. Comparison of Young's modulus obtained from experiments and oriented Mori-Tanaka calculations with and without voids at 120°F

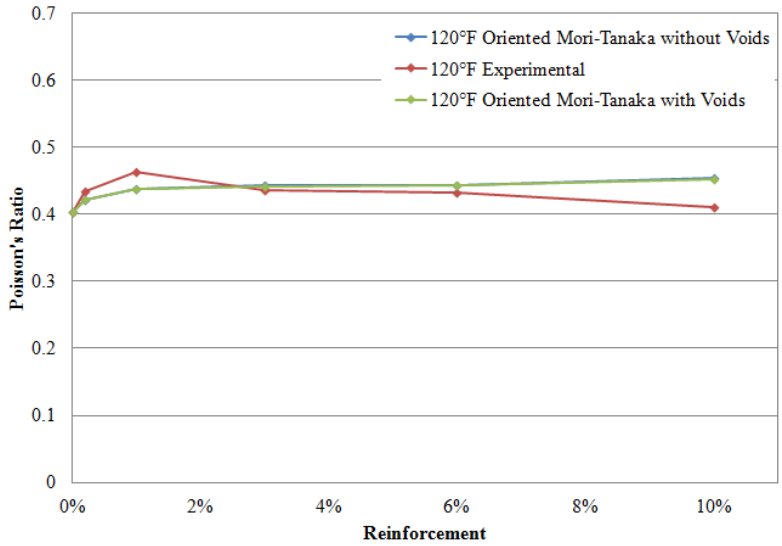

Figure 11. Comparison of Poisson's ratio obtained from experiments and oriented Mori-Tanaka calculations with and without voids at 120°F

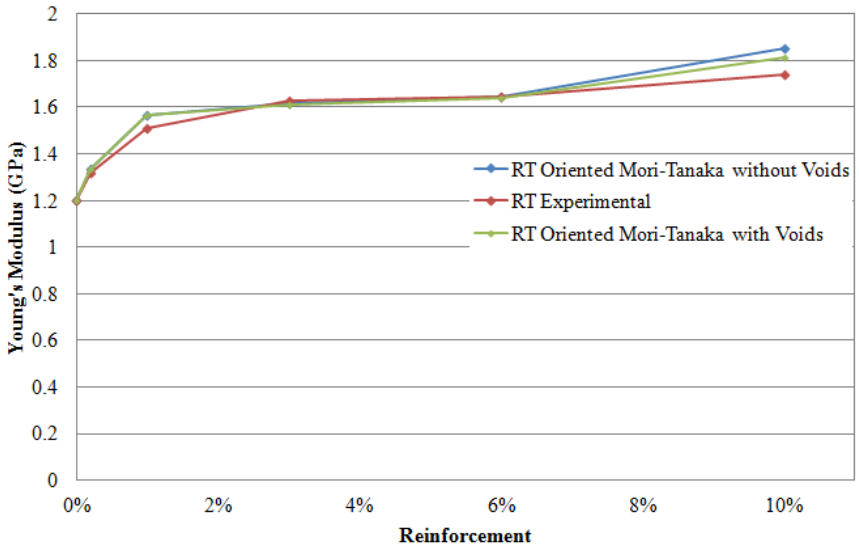

Figure 12. Comparison of Young's modulus obtained from experiments and oriented Mori-Tanaka calculations with and without voids at RT

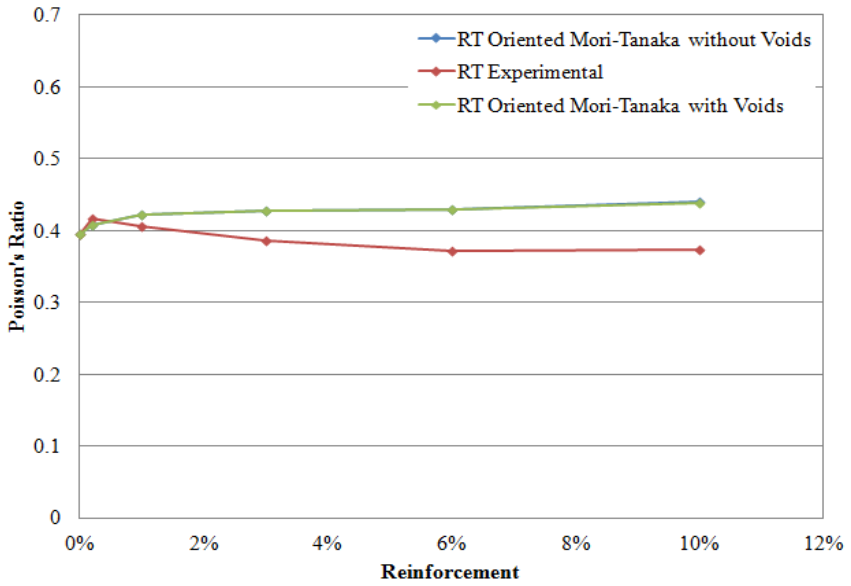

Figure 13. Comparison of Poisson's ratio obtained from experiments and oriented Mori-Tanaka calculations with and without voids at RT

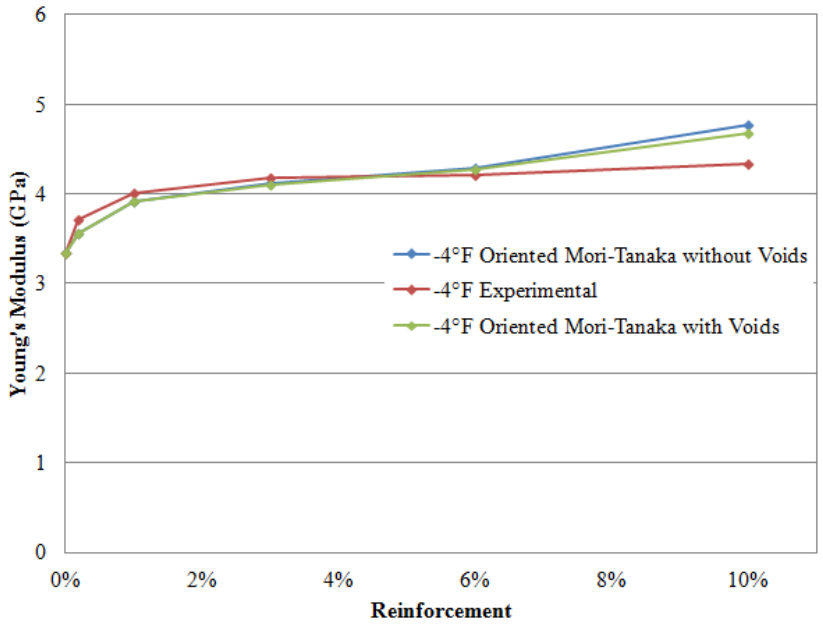

Figure 14. Comparison of Young's modulus obtained from experiments and oriented Mori-Tanaka calculations with and without voids at -4°F

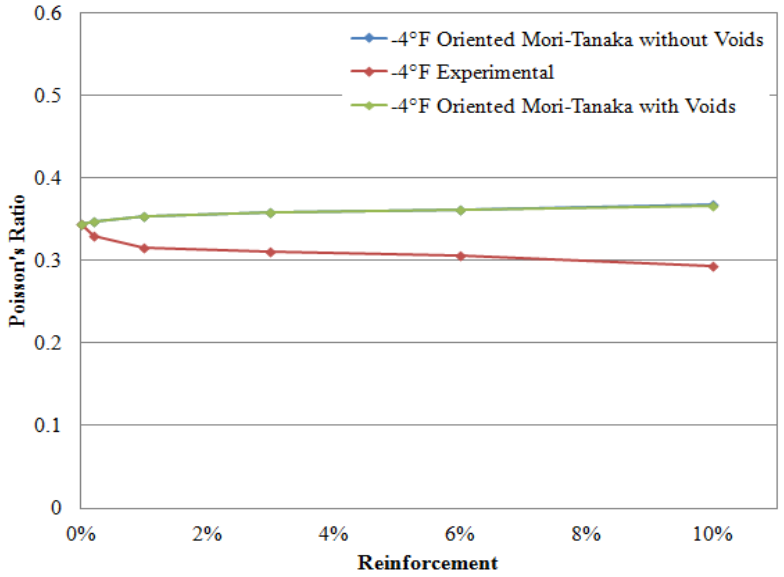

Figure 15. Comparison of Poisson's ratio obtained from experiments and oriented Mori-Tanaka calculations with and without voids at -4°F

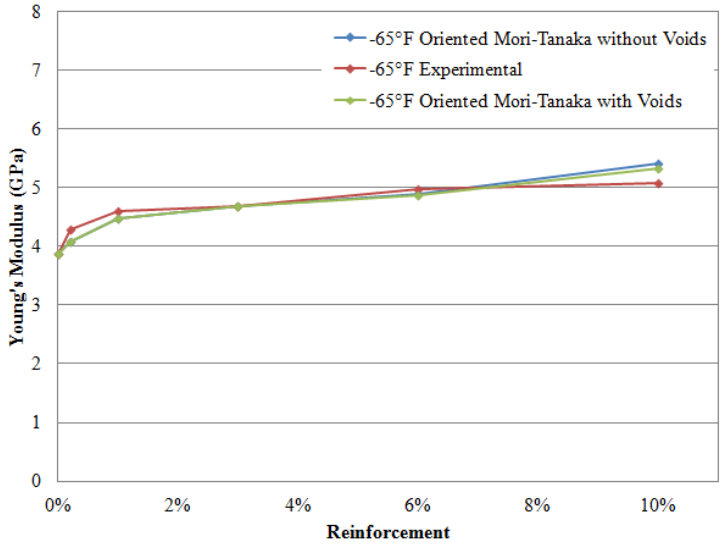

Figure 16. Comparison of Young's modulus obtained from experiments and oriented Mori-Tanaka calculations with and without voids at -65°F

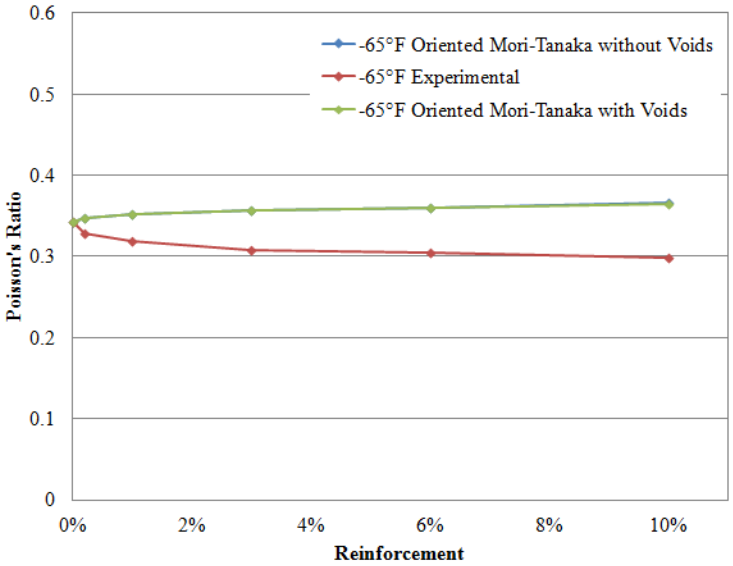

Figure 17. Comparison of Poisson's ratio obtained from experiments and oriented Mori-Tanaka calculations with and without voids at -65°F

As the results given in the previous figures indicate, the inclusion of voids in the calculations affects the value of Young's modulus mainly at 10% reinforcement but it does not affect the Poisson's ratio significantly. The results obtained by including the effect of voids in general give a better match with experimental data. At reinforcement percentages below 10% in some cases the curves obtained from the calculations including voids are indistinguishable from those without voids.

2.2-2) 2-D and 3-D Randomly Distributed Nanoclay Particles with Effect of Voids

First we recalculated the Mori-Tanaka results for the 2-D random cases by including the effect of voids and compared the results with experimental and 2-D random calculations without voids.

Next, the Mori-Tanaka calculations were repeated for the 3-D random cases by including the effect of voids, and compared with those obtained experimentally and from calculations without the effect of voids. For both cases the effect of voids on the mechanical properties was insignificant. Since the curves are similar to those shown in Figures 8-17, they are not presented here.

2.3 Temperature Effects

Figures 3.(a)-(e) show that especially at the higher temperatures the Mori-Tanaka results for oriented particles do not match the experimental results well.

Since nanoclay reinforced PP specimens don't show a pronounced linear material behavior at the higher temperatures and Mori-Tanaka calculations depend on linear material properties, we decided to include the temperature effect into the Mori-Tanaka calculations for 120°F and 160°F by redefining the Young's modulus.

At room temperature we have a clear linear behavior for low strains (or stresses) and we can calculate the elastic energy density per volume by considering the linear part of the curve. But when we perform the tensile tests at higher temperatures the linear portion of the curve is less pronounced and the curve is more or less nonlinear (see for example Figure 18. showing the initial part of a stress-strain at 160°F).

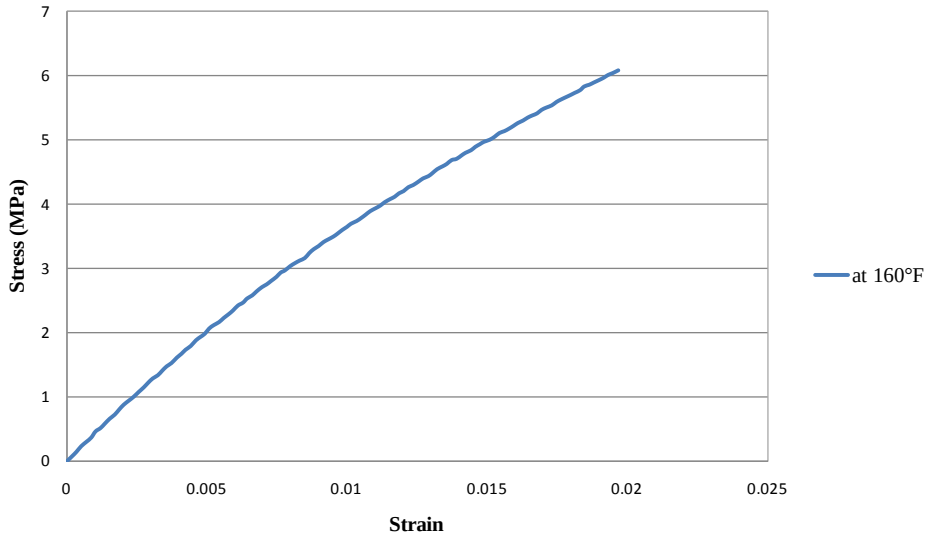

Figure 18. Initial part of stress-strain curve at 160°F

Considering the nonlinear behavior of the material, at high temperatures we believe that it is more appropriate to use the secant rather than the tangent in calculating the Young's modulus.

To calculate the Young's modulus at 120°F and 160°F we assume that the elastic energy density (recoverable energy) used to calculate the Young's modulus at room temperature is the same at high temperatures.

Figure 19.(a) and (b) show schematically the secant line and the elastic energy density using the stress-strain curves at 120°F and 160°F.

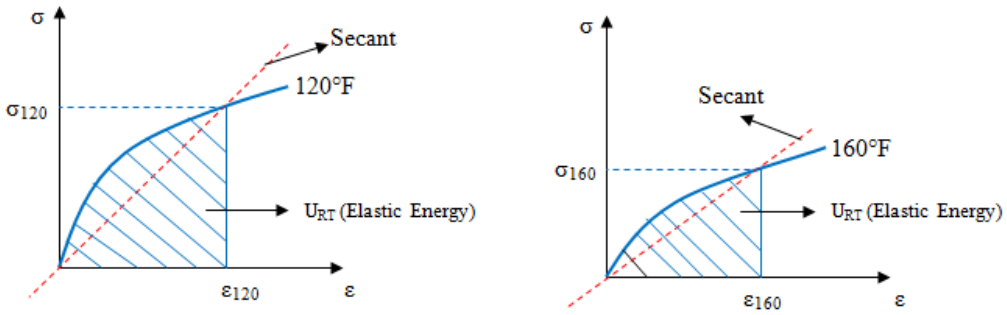

Figure 19. Calculation of secant Young's modulus from nonlinear material curve at (a) 120°F and (b) 160°F

First we calculate the strain energy density from the linear portion of the stress-strain curve at room temperature and then use this elastic energy to determine the strain (or stress) to be used in the calculation of the secant Young's modulus at higher temperatures.

Using this procedure we recalculated the Young's modulus of neat PP specimens at 120°F and 160°F based on the secant line as (Figure 19) : $E_{120} = \frac{\sigma_{120}}{\varepsilon_{120}}$; $E_{160} = \frac{\sigma_{160}}{\varepsilon_{160}}$ and we used these new values in the Mori-Tanaka formulas given in Eqs (3)-(8) and the composition assumed in Table 2 to calculate the elastic properties.

This temperature effect assumption was considered only for oriented particles in the Mori-Tanaka calculations.

Tables 10. and 11 show the Young's modulus values obtained experimentally and from Mori-Tanaka calculations using both the tangent and secant definitions at 120°F and 160°F respectively. It is noted that there is no significant effect when comparing the Young's modulus whether the results have been obtained from the tangent or secant calculations.

Table 10. Young's modulus values based on tangent and secant calculations at 120°F

120°F	YM Exp. (GPa) (Tangent)	YM Mori- Tanaka Without Temperature Effect (GPa) (Tangent)	YM Exp (Secant) (GPa)	YM Mori-Tanaka With Temp. Effect (GPa) (Secant)
0%	0.61595	0.61595	0.61389	0.61389
0.2%	0.7285	0.7079	0.72561	0.7057
1%	0.7646	0.85319	0.76208	0.85054
3%	0.8283	0.86217	0.82759	0.85941
6%	0.8332	0.8664	0.8328	0.8635
10%	0.8664	0.9789	0.85936	0.9757

Table 11. Young's modulus values based on tangent and secant calculations at 160°F

160°F	YM Exp. (GPa) (Tangent)	YM Mori- Tanaka Without Temperature Effect (GPa) (Tangent)	YM Exp (Secant) (GPa)	YM Mori-Tanaka With Temp. Effect (GPa) (Secant)
0%	0.39204	0.39204	0.38639	0.38639
0.2%	0.4499	0.4586	0.44771	0.4522
1%	0.4654	0.4654	0.46195	0.55355
3%	0.4969	0.4969	0.48835	0.55199
6%	0.5031	0.5583	0.50229	0.5504
10%	0.5146	0.632	0.51415	0.623

2.3 FINITE ELEMENT MODELING FOR TENSILE TESTING

A 3-D Finite Element model of the nanocomposite was developed using ABAQUS software. The 3-D model is based on the concept of representative volume element of the material.

The representative volume element has dimensions of (40units) x (40units) x (40units) and includes the matrix and oriented disk shaped particles (parallel to the loading direction) as shown in Figure 20. The number of particles n is adjusted to result in a fixed $\square/\square$ aspect ratio (used in the Mori-Tanaka calculations) and the desired nanoclay reinforcement percentage which varies from 0.2% to 10%.

To demonstrate how the various particle paramaters are calculated, consider the case for 0.2% nanoclay reinforcement. For 0.2% reinforcement, the volume fraction of nanoclay, using Eq.(2) or Table 1., is 0.095%.

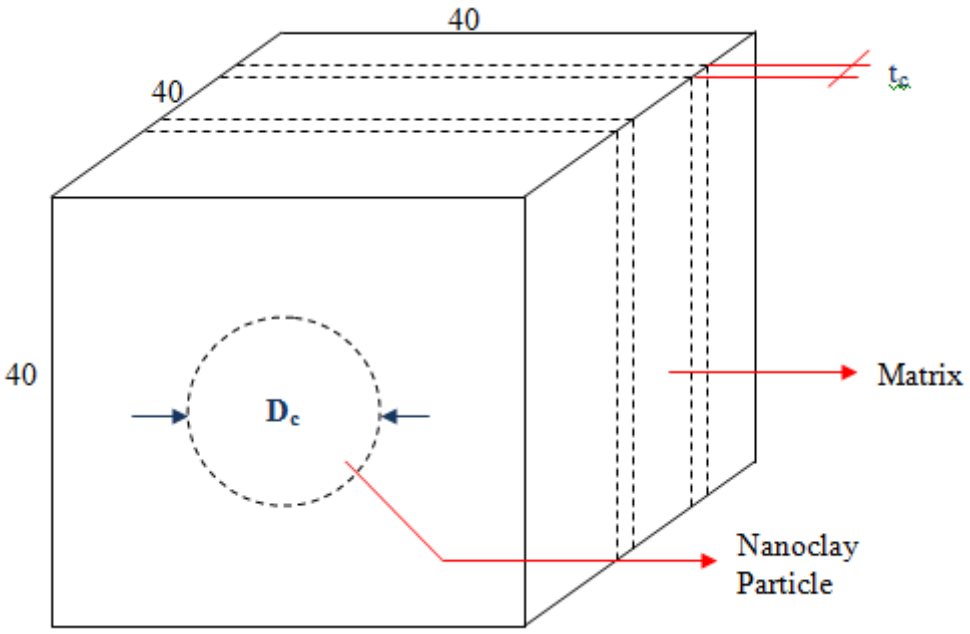

Figure 20. Representative Volume Element

In the previous section for 0.2% the disk diameter and particle thickness were assumed as: D=200nm and t=0.615 nm.

Thus, $\frac{t}{D}=\frac{0.615}{200}$ or D=325.20t.

To maintain the same aspect ratio, we write;

$\frac{t_c}{D_c}=\frac{t}{D}=\frac{1}{325.20}$ or $D_c=325.20t_c$

Then, assuming n=2 and the total volume as V, from the volume fraction equation t_c is found as:

$$c=\frac{n\frac{\pi D_c^{\,2}}{4}t_c}{V} \qquad (65)$$

or

$$0.00095=\frac{2\pi\left(325.20\right)^2 t_c^{\,3}}{4\left(40\right)^3}\rightarrow t_c=0.0715 \text{ units and } D_c=23.25 \text{ units.}$$

For 6% and 10%, t_c and D_c are calculated similarly. For 1% and 3%, since we have particles of different thicknesses the calculation, though in principle the same, is slightly different. To illustrate this, consider the case of 1% reinforcement.

As explained in section 2 and Table 2, for 1% we use a combination of particles with different thicknesses. The composition used was 40% of N=1 particles, 30% of N=2 particles and 30% of N=3 particles. The volume fraction c corresponding to 1% is 0.48% (Table 1).

Again, to maintain the same aspect ratios used previously, we calculate the particle thicknesses as follows:

- For N=1 particles, D=200 nm, t=0.615 nm or D=325.20t. If we assume 2 layers with particles of this geometry, then with $D_c=325.20t_c$ we obtain:

$$\frac{2\pi(325.20)^2 t_c^{\,3}}{4(40)^3} = 0.4(0.0048) \rightarrow t_c = 0.0904 \text{ units and } D_c = 29.41 \text{ units.}$$

- For N=2 particles, D=200 nm, t=3.015 nm or D=66.33t. If we assume 2 layers with particles of this geometry, then with $D_c=66.33t_c$ we obtain:

$$\frac{2\pi(66.33)^2 t_c^{\,3}}{4(40)^3} = 0.3(0.0048) \rightarrow t_c = 0.2371 \text{ units and } D_c = 15.73 \text{ units.}$$

- For N=3 particles, D=200 nm, t=5.415 nm or D=36.93t. If we assume 1 layer with particles of this geometry, then with $D_c=36.93t_c$ we obtain:

$$\frac{\pi(36.93)^2 t_c^{\,3}}{4(40)^3} = 0.3(0.0048) \rightarrow t_c = 0.4414 \text{ units and } D_c = 16.30 \text{ units.}$$

The calculations for 3% are similar to those presented above. The calculated particle parameters for each reinforcement percentage are given in Table 12.

Table 12 The particle parameters used in the finite element calculations for each reinforcement percentage

Reinforcement Percentage	n	t_c	D_c
0.2%	2	0.0715	23.25
1%	2	0.0904	29.41
	2	0.2371	15.73
	1	0.4414	16.30
3%	2	0.3764	24.97
	2	0.5053	18.66
	1	0.8131	20.81
6%	6	1.0125	19.82
10%	10	1.1747	18.62

To explain the methodology used in the finite element model, consider the case for 0.2% reinforcement. Here, we have 2 layers with nanoclay particles, in the PP matrix. Figure 21 shows the symmetric finite element model constructed for this case. The bottom surface was constrained in y-direction and one point in the middle of the bottom surface was fixed to prevent translational displacement. The side surfaces were assumed stress free.The boundary conditions and loading are shown in Figure 4.60. For loading, a unit displacement was applied at the top surface.

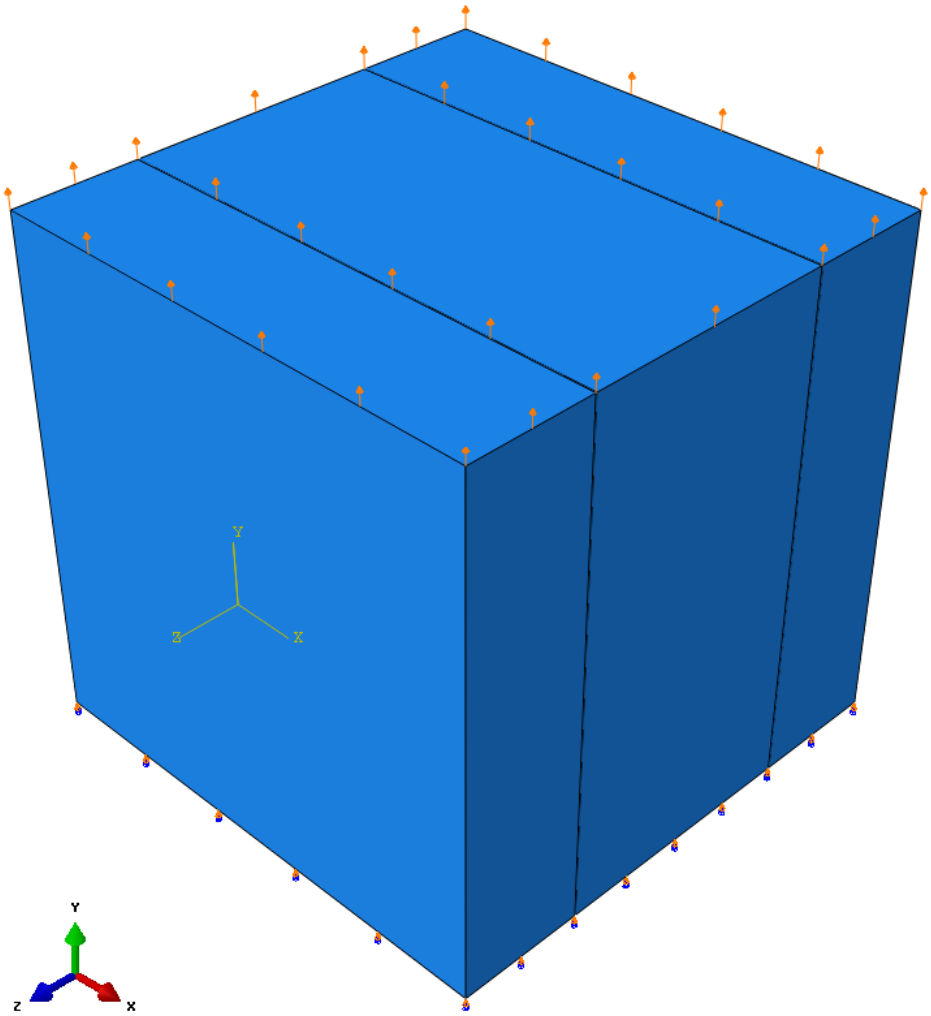

Figure 21 The boundary conditions and displacement loading for the 0.2% specimens

The 3-D finite element mesh is shown in Figure 22.

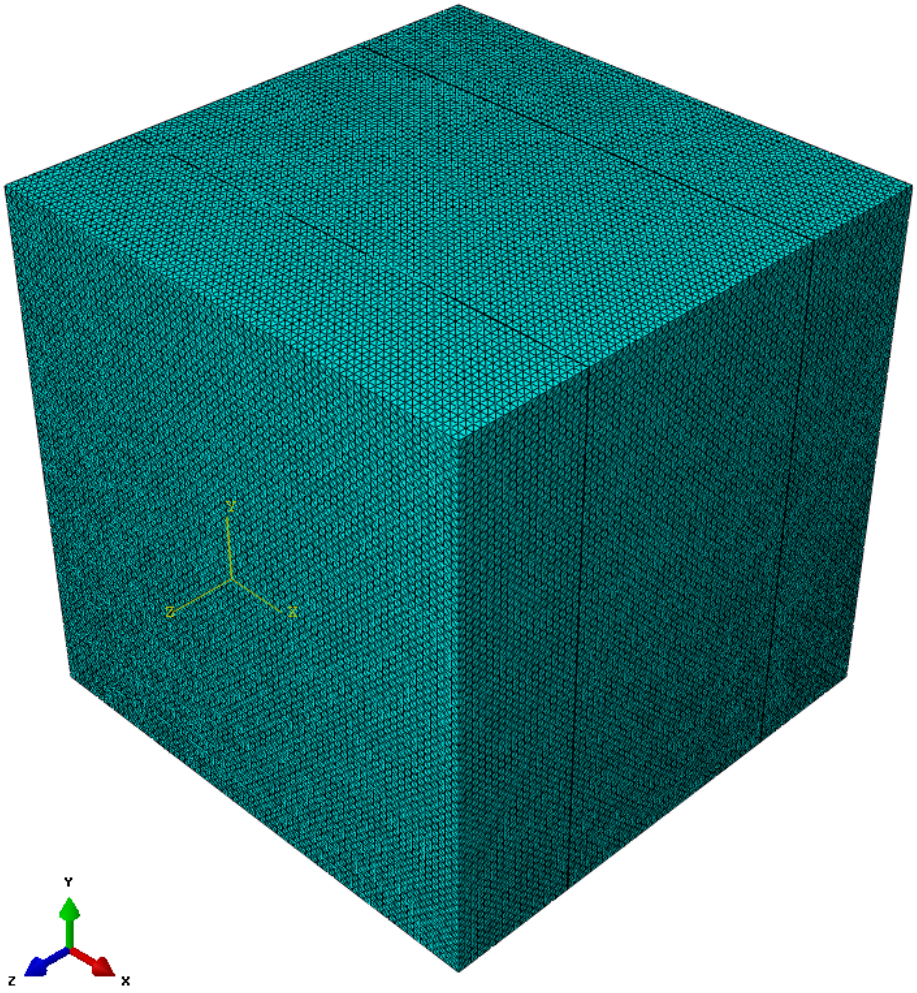

Figure 22 The mesh structure of the finite element model

The Young's modulus and the Poison's ratio are obtained using the total force (F) at the top surface and the calculated values of, σ_y , ε_x and ε_y as shown below:

$$\sigma_y = \frac{Total\ Force}{Area} = \frac{F}{40x40}$$

$$\varepsilon_x = \frac{(\Delta u)_{average}}{40}$$

and

$\varepsilon_x = \frac{1}{40}$,

$E = \frac{\sigma_y}{\varepsilon_y}$

and

$\vartheta_{12} = -\frac{\varepsilon_x}{\varepsilon_y}$

The Young's modulus and the Poisson's ratio were calculated using the finite element technique for all percentages, namely 0.2%, 1%, 3%, 6% and 10% at -65°F, -4°F and RT. The finite element results for Young's modulus and the Poisson's ratio are summarized in Tables 13 and 14 respectively and compared with those obtained from experiments and the Mori-Tanaka calculations for oriented particles.

Table 13. Comparison of E/E_m values obtained from experiments, Mori-Tanaka and FEM calculations at various temperatures

	E/E_m			
Reinforcement Percentage of PP 3371	**Temperature**	**Experimental**	**Mori-Tanaka Calculation (Oriented)**	**FEM**
0.2%	*-65ºF (-54ºC)*	1.1083	1.0551	1.0489
	-4 ºF (-20ºC)	1.1095	1.0612	1.0539
	Room Temp.	1.0976	1.1148	1.0945
1%	*-65ºF (-54ºC)*	1.1909	1.1559	1.1390
	-4 ºF (-20ºC)	1.1977	1.1722	1.1521
	Room Temp.	1.2569	1.3048	1.2544
3%	*-65ºF (-54ºC)*	1.2146	1.2118	1.1757
	-4 ºF (-20ºC)	1.2487	1.2289	1.1877
	Room Temp.	1.3564	1.3458	1.2668
6%	*-65ºF (-54ºC)*	1.2867	1.2498	1.2066
	-4 ºF (-20ºC)	1.2587	1.2638	1.2162
	Room Temp.	1.3718	1.3443	1.2751
10%	*-65ºF (-54ºC)*	1.3174	1.4023	1.2452
	-4 ºF (-20ºC)	1.2948	1.4239	1.2533
	Room Temp.	1.4520	1.5455	1.3055

Table 14. Comparison of ν_{12}/ν_m values obtained from experiments, Mori-Tanaka and FEM calculations at various temperatures

	ν_{12}/ν_m			
Reinforcement Percentage of PP 3371	**Temperature**	**Experimental**	**Mori-Tanaka Calculation (Oriented)**	**FEM**
0.2%	*-65ºF (-54ºC)*	0.9574	1.0111	0.9798
	-4 ºF (-20ºC)	0.9618	1.0125	0.9869
	Room Temp.	1.0557	1.0317	0.9742
1%	*-65ºF (-54ºC)*	0.9311	1.0281	0.9813
	-4 ºF (-20ºC)	0.9179	1.0312	0.9805
	Room Temp.	1.0276	1.0681	0.9764
3%	*-65ºF (-54ºC)*	0.8970	1.0388	0.9725
	-4 ºF (-20ºC)	0.9057	1.0425	0.9724
	Room Temp.	0.9759	1.0813	0.9724
6%	*-65ºF (-54ºC)*	0.8863	1.0462	0.9956
	-4 ºF (-20ºC)	0.8888	1.0497	0.9974
	Room Temp.	0.9429	1.0815	1.0106
10%	*-65ºF (-54ºC)*	0.8699	1.0665	1.0382
	-4 ºF (-20ºC)	0.8516	1.0713	1.0418
	Room Temp.	0.9437	1.1140	1.0689

The results are also depicted in Figures 23-28.

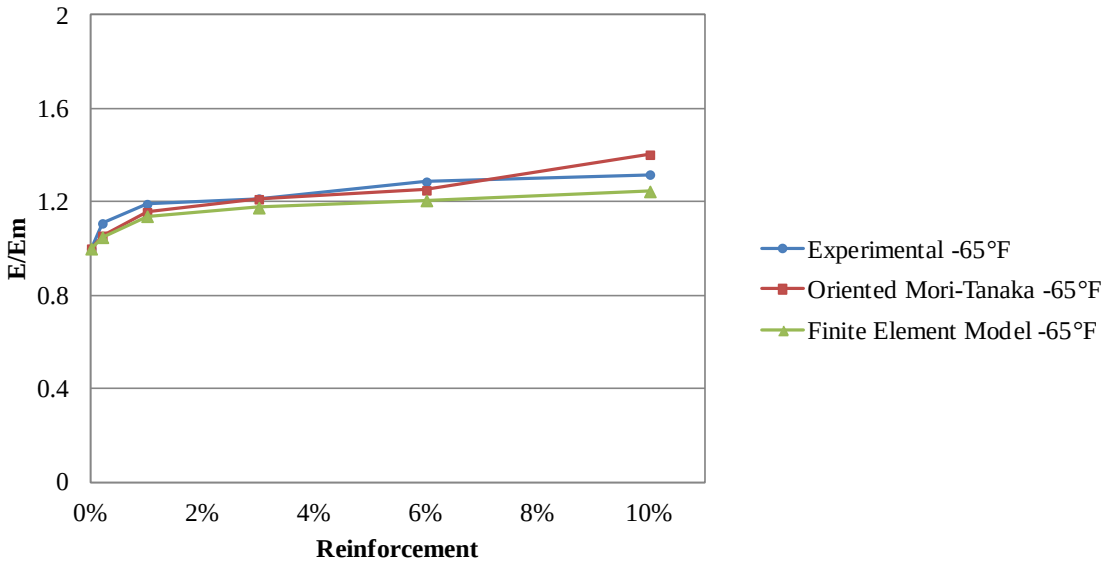

Figure 23. Comparison of E/E_m values obtained from the experiments, Mori-Tanaka calculations and the finite element model at -65°F

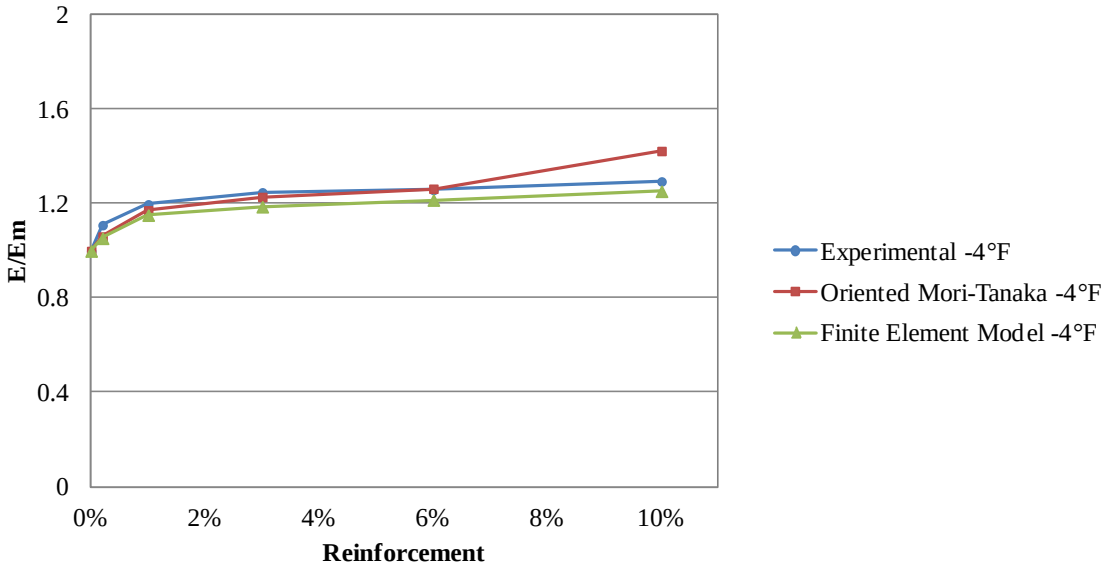

Figure 24. Comparison of E/E_m values obtained from the experiments, Mori-Tanaka calculations and the finite element model at -4°F

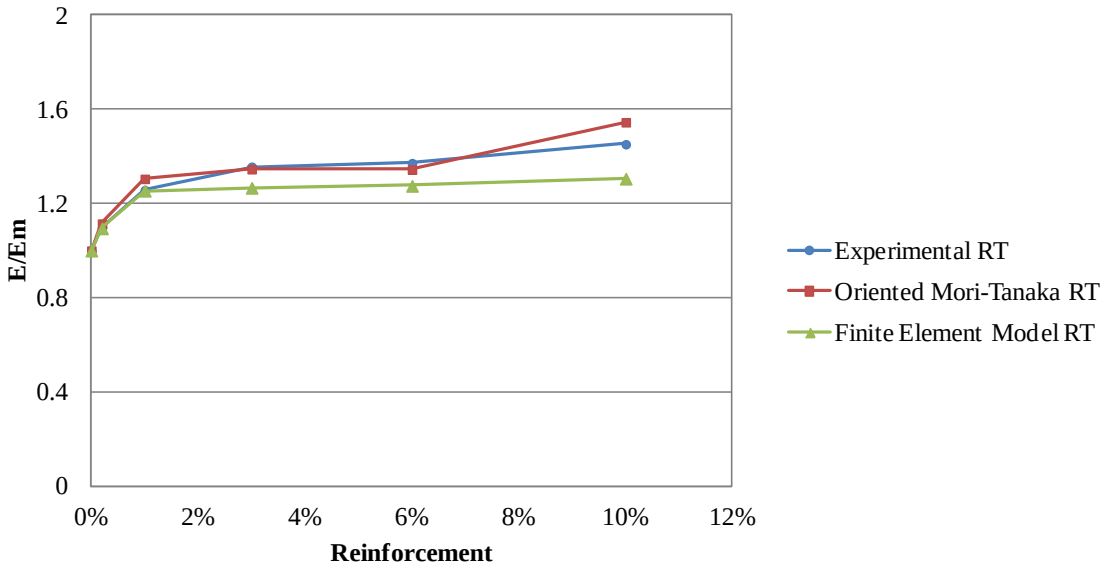

Figure 25. Comparison of E/E_m values obtained from the experiments, Mori-Tanaka calculations and the finite element model at room temperature

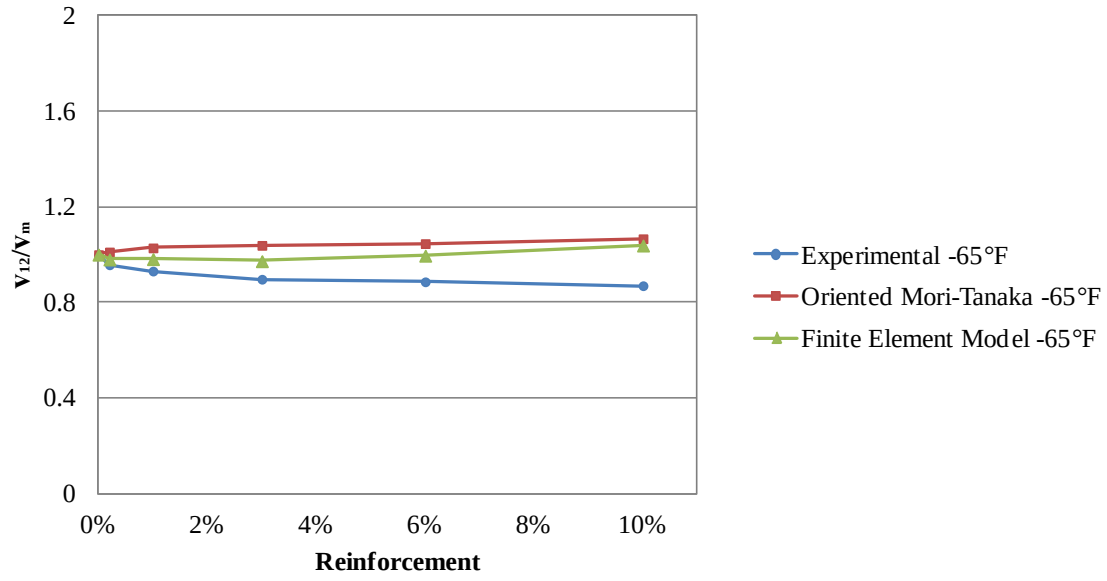

Figure 26. Comparison of ν_{12}/ν_m values obtained from the experiments, Mori-Tanaka calculations and the finite element model at -65°F

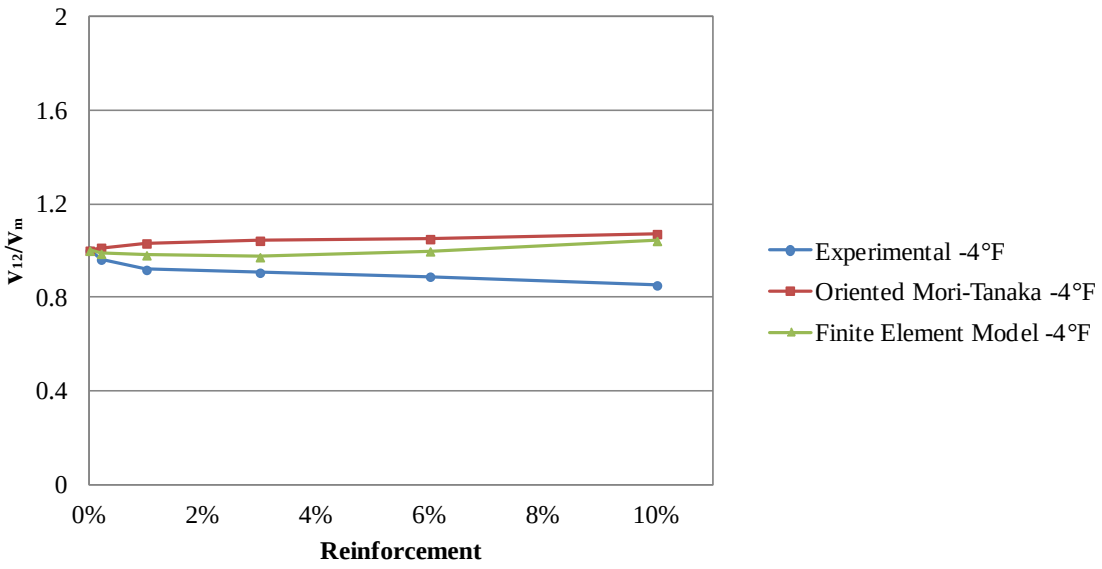

Figure 27. Comparison of v_{12}/v_m values obtained from the experiments, Mori-Tanaka calculations and the finite element model at -4°F

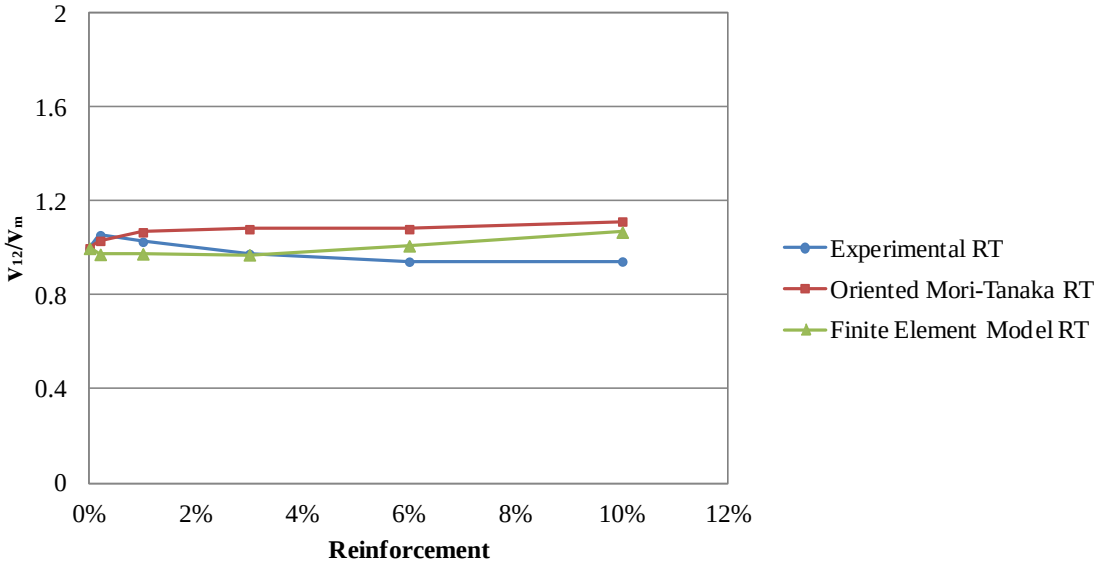

Figure 28. Comparison of v_{12}/v_m values obtained from the experimentally, Mori-Tanaka calculation and the finite element model at room temperature

The results given in Tables 13-14 and Figures 23-28 indicate that the finite element model may be also a good predictive tool to determine the elastic properties of nanoclay reinforced polymers.

3. DISCUSSION AND CONCLUSIONS

In this paper (Part II) the Mori-Tanaka formulation and the Finite Element Method (FEM) were used to predict the elastic properties of nanoclay reinforced PP composites at various temperatures. The Mori-Tanaka formulation was modified to include particles of different thicknesses. Three different particle distributions, namely; a) oriented particles, b) 2-D randomly distributed particles and c) 3-D randomly distributed particles were compared to those obtained experimentally. As noted previously, the results in Figure 3. indicate that the Mori-Tanaka results match the experimental data reasonably well. It appears that the results for oriented particles provide the best match and the results for 2-D and 3-D randomly distributed particles are close to each other. The variation of mechanical properties with temperature, especially Young's modulus can be very significant (Figure 2). For example experimental data for 3% nanoclay reinforcement specimens show that the Young's modulus is reduced by 89% when the temperature increases from -65°F to 160°F (Figure 2.c). The bulk of this decrease takes place around the glass transition temperature (T_g) of PP. For example, the Young's modulus decreases by 61% when the temperature is raised from -4°F to RT. This change occurs because the matrix material PP changes from a glassy state to a rubbery state as it crosses T_g which is around 14°F. Similar trends are also observed for the other reinforcement percentages. We note that the Mori-Tanaka calculations captured these trends accurately in all cases. Even though it was difficult to experimentally determine the Poisson's ratios with precision, the Mori-Tanaka prediction provided satisfactory estimates (Figures 4 and 5).

The Mori-Tanaka formulations were also used to predict the elastic properties of epoxy based nanocomposites. The comparison of theoretical and experimental results for the Young's modulus and the Poisson'sratio is shown in Figures 6 and 7. For epoxy based composites there was significant difference between the predicted and experimental results. We believe this may be due to agglomeration of nanoclay particles in epoxy because of its higher viscosity.

The Mori-Tanaka formulations were modified to include the effects of voids and temperature. The results indicate that these effects become perceptible only at the highest reinforcement percentage and temperature (Figures 8-17 and Tables 10-11). Finally, a finite element (FE) model based on the representative volume concept was developed to predict the Young's modulus and Poisson's ratio of the composite. The results obtained from the finite element calculations were compared with the experimental data and the results obtained from the Mori-Tanaka formulations for oriented particles (Figures 23-28). In general, the FE results match those obtained previously (experimental and Mori-Tanaka), except at 10% reinforcement.

In light of these results, one may deduce the following conclusions:

a. With a proper choice of geometric and material properties for the constituents, the Mori-Tanaka formulation may be a good tool in predicting the Young's modulus. The Mori-Tanaka results, especially those obtained for oriented particles, matched well with the experiments, except at high temperatures and high reinforcement percentages

b. Inclusion of voids in the Mori-Tanaka formulation gave a somewhat better match with experimental data at higher reinforcement percentages

c. The effect of temperature was included by using the secant instead of the tangent in calculating the Young's modulus. As a consequence, better match with experiments was obtained at higher temperatures.

d. The 3-D finite element model also provides a good estimate for the Young's modulus of the nanocomposite. As the results displayed in the figures show, the finite element results compare well with those obtained experimentally.

REFERENCES

[1] Bayar, S., Delale, F. and Liaw, B., "Effect of Temperature on Mechanical Properties of Nanoclay Reinforced Polymeric Nanocomposites – Part I: Experimental Results".

[2] Sheng, N., Boyce, M.C., Parks, D. M., Rutledge, G.C., Abes, J. I.,Cohen, R.E., Multiscale Micromechanical Modeling of Polymer/Clay Nanocomposites and The Effective Clay Particle, Polymer 45, 2004, pp. 487-506.

[3] Nam PH, Maiti P, Okamoto M, Kotaka T, Hasegawa N, Usuki A. Polymer 2001;42:9633

[4] Van Es M, Xiqiao F, van Turnhout J, van der Giessen E. In: Al-Malaika S, Golovoy A, Wikie CA, editors. Specialty Polymeradditives. Malden, MA: Blackwell Science; 2001.

[5] Brune DA, Bicerano J. Polymer 2002;43:369.

[6] Yoon PJ, Fornes TD, Paul DR. Polymer 2002;43:6727.

[7] Fornes T.D., Paul D.R., Polymer, Volume 44, 2003, Pages 4993-5013.

[8] Drozdov A.D., Lejre A.H., Christiasen J., Viscoelasticity, viscoplasticity, and creep failure of polypropylene/clay nanocomposites, Composites Science and Technology, Volume 69, 2009, Pages 2596-2603.

[9] Nguyen Q. T., Process for Improving Exfoliation and Dispersion of Nanoclay Particles into Polymer Matrices Using Supercritical Carbon Dioxide. PhD. Dissertation , Blacksburg, VA, 2007.

[10] J.C Halpin, J.L Kardos, The Halpin-Tsai Equations: A Review. *Polym. Eng. Sci.* 16 (1976), pp. 344.

[11] T.D. Fornes, D.R. Paul, Modeling properties of nylon 6/clay nanocomposites using composite theories. *Polymer Eng. Sci.* 44(2003), pp. 4993.

[12] Bayar S., *An Experimental and theoretical Study of the Effect of Temperature on The Mechanical Behavior of Nanoclay Reinforced Polymers*. PhD Dissertation, CUNY, NY, 2012.

[13] Lee H, Cohen RE, McKinley GH. (Manuscript in preparation; see [2])

[14] Pantano A, Parks DM, Boyce MC. J Mech Phys Solids 2003.

[15] Tandon, G. P., and Weng, G. J., The Effect of Aspect Ratio of Inclusions on the Elastic Properties of Unidirectionally Aligned Composites, Polymer Composites, October 1984, Vol. 5, No. 4.

[16] Tandom, G. P., Weng, G. J., Average Stress in the Matrix and Effective Moduli of Randomly Oriented Composites, Composite Science and Technology, 27, 1986, pp. 111-132.